LBL-10586 c.2
Preprint

Lawrence Berkeley Laboratory
UNIVERSITY OF CALIFORNIA

Accelerator & Fusion
Research Division

Submitted to The Physics of Fluids

THE TORMAC V EXPERIMENT

I.G. Brown, B. Feinberg, W.B. Kunkel, M.A. Levine,
R.A. Niland, R.S. Shaw, and B.G. Vaucher

March 1980

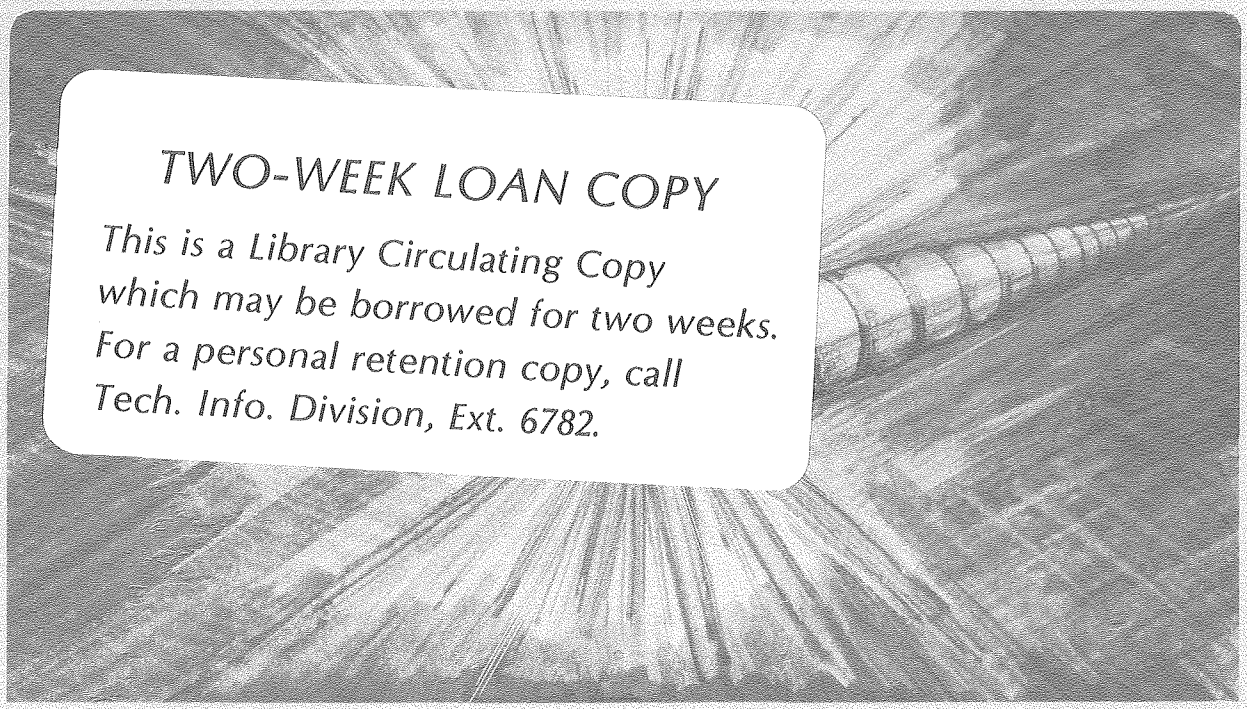

Prepared for the U.S. Department of Energy under Contract W-7405-ENG-48

DISCLAIMER

Submitted to Phys. of Fluids LBL-10586

THE TORMAC V EXPERIMENT*

I. G. Brown, B. Feinberg, W. B. Kunkel, M. A. Levine,
R. A. Niland,+ R. S. Shaw and B. G. Vaucher++

Lawrence Berkeley Laboratory, University of California
Berkeley, California 94720

March 1980

ABSTRACT

Tormac (Toroidal Magnetic Cusp) is a plasma confinement concept combining the favorable MHD stability properties of a cusp geometry with the good particle confinement inherent to closed field geometry. A Tormac plasma has two regions: an interior region in which a toroidal bias or stuffing field is embedded, and an exterior or surface region confined by mirror trapping along open field lines. The combination of these two regions is expected to lead to a configuration having confinement substantially superior to that of a mirror, and to allow the plasma to be stable at high β. The Tormac V experiment is an attempt to establish such a configuration and to investigate the characteristic behavior of the Tormac plasma.

In this paper we describe the Tormac concept, the Tormac V experimental set-up, and the results obtained.

*Work supported by U. S. Department of Energy, Office of Fusion Energy, under contract W-7405-ENG-48.
+ Present address: University of Sydney, Sydney, NSW, Australia.
++Present address: University of Fribourg, Switzerland

I. Introduction

Tormac V is a toroidal bicusp plasma confinement device constructed to test the Tormac concept in the collisionless regime. Briefly, as the plasma was heated in successive experiments, we hoped to see: first of all a decrease in confinement time as plasma was lost more rapidly through the cusps by collisional processes. Then, when the plasma became collisionless ($\lambda_i > r_p$), a turn-around and an increase of confinement time with T_i, indicating that the plasma was being trapped by mirror confinement on the open field lines at the cusps. We were also interested in the plasma stability properties, particularly the stability and characteristic behavior of the sheath.

This paper first summarizes the Tormac confinement concept. Then, the experimental facility and diagnostic array are described. Next, we discuss the ionization phase of the discharge, before the main Tormac bicusp magnetic field is applied, and then our observations of the plasma behavior during the main Tormac confinement period. Finally, we summarize our measurements and interpretations.

Our basic conclusion is that the Tormac configuration was not achieved. The plasma was of density $\sim 2 \times 10^{15}$ cm^{-3} and temperature ~ 5 - 10 eV. Separation of magnetic field in the interior plasma region from the external, confining field was not obtained; a sharp, quasi-steady sheath was not established.

II. The Tormac Concept

Tormac is a stuffed, toroidal, line cusp.[1-3] Plasma is contained in two distinct regions - an interior, high ß region lying entirely on field lines closed within the plasma and an outside or sheath region where the magnetic field lines are open. Particles within

the sheath region are confined in a mirror-like fashion by magnetic field constrictions some distance beyond the cusp lines[3] (Fig. 1). In the steady state, plasma from the interior region enters the sheath region at the same rate at which it is lost from the sheath. This means that plasma particles must join the sheath roughly at the ion scattering rate N_s/τ_i,[4] where N_s is the number of particles in the sheath volume and τ_i is the ion scattering time. Since the interior volume can be made much larger than the sheath volume, the overall device confinement time is expected to be greater than that of the sheath region alone (mirror confinement) by the ratio of the number of particles in the interior region to the number of particles in the sheath region. For reactor parameters[5] this ratio can be of order 10-100, and so also is the factor by which Tormac confinement is improved over pure mirror confinement.

The line cusp can be of arbitrary order, but there are engineering advantages associated with a toroidal two-pole cusp as opposed to a four-pole or higher order cusp (ease of mechanical and electrical fabrication); the experimental device is a two-pole cusp - the Tormac bicusp. The conceptual plasma and field shape are indicated in Fig. 1. The field at the plasma surface consists of poloidal and toroidal components combined in such a manner as to give rise to the indicated shape when the interior region contains plasma at high ß, and to satisfy the basic cusp condition of favorable magnetic field curvature everywhere on the surface. This is accomplished by having the magnetic field on the inside of the torus dominated by the toroidal component and the magnetic field on the outside of the torus dominated by the poloidal component.

The plasma surface is thus stabilized by the absolute minimum-B field. At the same time the interior region is also expected to be MHD stable, since unlike many other devices and characteristic of high ß cusp confinement, the interior region is a region with only minor pressure gradients; the pressure profile is almost flat in the interior region, with essentially all the plasma pressure being supported by the steep field gradient in and near the sheath.

In the Tormac V experiment, we wish to form a toroidal plasma having an imbedded toroidal magnetic field and also a toroidal current, as part of the ionization process. The poloidal field due to the plasma current gives a rotational transform to the field within the plasma. The "cusp field" - by which we mean the combination of poloidal and toroidal fields which together form the required Tormac configuration of surface field geometry - is then switched on, rising to full value of $\lesssim 5$ kG in a time of about 13 μsec. This compresses the pre-existing plasma into a new equilibrium - the Tormac equilibrium. After compression two regions exist: a Maxwellian plasma on closed field lines having a rotational transform and a magnitude of order 1 kG, and a mirror confined sheath plasma on a mixture of poloidal and toroidal components having a magnitude $\lesssim 5$ kG. As this configuration evolves, the two regions are maintained, with the sheath region diffusing into the bulk plasma on the scale of the Tormac confinement time. At the plasma surface, magnetic and particle pressures are balanced, and there is a strong magnetic shear and a high density gradient.

An essential part of the experimental program was to investigate to what extent the above picture is obtained in the laboratory.

III. Experimental Set-Up

A. Device Description

Tormac V was designed to correct two conditions that were thought to be a problem in Tormac IV: (i) a large vessel was used so as to increase the volume to surface ratio and so reduce background impurities, (ii) the vessel was constructed so that the open field lines forming the cusp mirrors were long and were located inside the vessel - i.e., the peak of the magnetic mirror field, going out along the cusp line, occurred in the vacuum. Also, the magnetic field was made to flare out so that the intensity was low where it intersected the wall. This was done so as to reduce local heating due to out-flowing plasma, and to increase the length of the open field lines, so that backflowing cold gas or plasma would not reach the sheath and main body of plasma until after the period of main experimental interest. The shape of the vessel and the expected plasma location and cusp field shape are shown in Fig. 2.

The vessel is constructed from pyrex glass of thickness varying from 0.5" to 1.5"; discs and cylinders were epoxied together to form the required shape. Maximum tensile stress was designed to be no greater than about 1000 psi, and a test pump-down with many strain gauges attached indicated stresses below this limit. The vessel is 1 m diam x 1 m long and its volume is $\sim 340\ell$, or $\sim 450\ell$ including the pumping pipes; the design post-compression plasma volume is $\sim 45\ell$. The system is pumped with a speed of 260 ℓ/sec and a base pressure of $\sim 1 \times 10^{-7}$ Torr at the pump; at the vessel the speed is ~ 80 ℓ/sec and the base pressure $\sim 5 \times 10^{-7}$ Torr. The filling gas was usually an

80:20 hydrogen/helium mix, with some runs with pure hydrogen or deuterium; helium was added for spectroscopic diagonostics. A few seconds before a shot is to be made, the vessel is valved off from the pump and a known amount of gas puffed in, raising the pressure to a predetermined value, typically 5-50 mTorr. In this way, the rise in background gas pressure is minimized, maximizing gas purity.

After the introduction of gas, the discharge sequence is initiated. The first capacitor bank fired is to establish the quasi-d.c. (for the duration of the experiment) toroidal bias field. This field rises to a peak value of up to ~ 800 G in a time ~ 250 μsec. At this time, or slightly earlier, the ionize bank is fired.

The gas is ionized and a toroidal current set up via a set of toroidally wound coils surrounding the vessel at various locations, driven from the ringing discharge of a capacitor bank. The ionize coils and ionize capacitor bank underwent a number of changes in the course of the experiment, but typically the capacitor bank was of energy 10-40 kJ and discharged through the coils with a ringing frequency ~30-50 kHz, inducing a toroidal plasma current of magnitude ~25-100 kA. The design philosophy and experimental observations of the ionize phase are discussed in the next section.

Some tens of microseconds after the ionize bank is fired and a current-carrying equilibrium toroidal plasma has been established, the main bank (called the cusp bank) is discharged into the main windings (cusp windings). The confining magnetic field in Tormac V was designed as a bicusp. This field has an absolute minimum-B which requires both toroidal and poloidal components, and the device was wound with a single

coil having both poloidal and toroidal components; there are 132 wires in parallel distributed over the surface of the vessel, and these are split into three series sections to allow a Marx-like operation of the main bank. This particular design - as opposed to having separate sets of windings for the poloidal and toroidal components - ensures that the ratio of poloidal to toroidal current remains constant throughout the pulse, keeping the magnetic geometry constant; it also minimizes coupling between the various coils. The shape of the windings on the surface of the vessel was initially designed using an electrolytic analog tank[6] and later improved by a computer analysis.[7] Plots of the calculated flux surfaces, $|B|$ surfaces, and of $|B|(R)$ at the midplane are shown in Figs. 3-5. The minimum-$|B|$ magnetic well is evident. The main field capacitor bank stores 160 kJ when charged to maximum operating voltage of 20 kV per each of the three series sections. When discharged into the windings, a current of up to 650 kA gives rise to a field of $\lesssim$ 5 kG at R = 25 cm, the design location of the inner surface of the plasma. The field rises with a quarter period of 13 μsec and is crowbarred with a decay time of several hundred microseconds.

A part of the experimental program was to investigate "shaker heating"[8,9] (magnetoacoustic wave heating). For this purpose a high power rf generator of the type pioneered by the Lausanne group[10] was constructed, consisting of a lumped delay line with individually switched sections. This generator delivers ~6 cycles at ~250-500 kHz, with a peak power of over 1 GW, into a single turn copper strap wrapped around the midplane circumference of the vessel.

The timing sequence is thus as follows: The bias bank is fired, establishing a toroidal stuffing field in the vessel which rises to a peak of $\lesssim$800 G in ~250 μsec and which is quasi-d.c. for the duration of the experiment. The ionize bank is then fired, which breaks down the gas and forms a toroidal plasma carrying a current of amplitude of $\lesssim$100 kA within a few tens of microseconds. Next, the cusp bank is discharged into the main Tormac windings, rising with a quarter period of 13 μsec to a peak field of $\lesssim$5 kG at the plasma location and crowbarred with a decay time ~400 μsec. At some time during or after the cusp field rise, the shaker heating bank may also be triggered.

B. Diagnostics

A 16 channel polychromator was used to measure line broadening as a function of space (line-of-sight) and time. Channels were 0.3Å apart and the resolution was about 0.3Å. A fiber-optic light pipe terminating at the polychromator entrance slit facilitated scanning the plasma in major radius. Because of the translucent nature of the outer glass cylinder of the vessel, it was possible to view the plasma radially only at the midplane, through a port located there. The output signals from the 16 channels were fed into our computer data acquisition system,[11,12] as were most other diagnostics, and spectral line shapes could be displayed and analyzed on the computer's video display unit immediately after each shot. These and other diagnostic data were recorded on magnetic tape, and we have permanent records that can be retrieved by the computer at any time.

Electron density integrated along a line-of-sight was measured from a feedback-stabilized Michelson, helium-neon (λ6328Å) interferometer. Depending on the level of laser ripple and acoustic

noise in the environment, the rms noise level of this instrument is $\sim 10^{-2}$ of a fringe, corresponding to a minimum detectable $\int n_e d\ell \sim 2 \times 10^{14} cm^{-2}$ or a mean density $\bar{n}_e \sim 10^{13}$ cm^{-3}. The interferometer is contained in a U-shaped fiberglass housing suspended from above the vessel and can be moved vertically to scan $\int n_e d\ell$ in the axial direction as a function of major radius.

Absolute measurements of the electron temperature and relative measurements of the electron density were made using 90° Thomson scattering of ruby laser light (λ6943Å). The Q-switched laser output is a pulse of 2-4 J with a width $\sim$25 nsec. The beam is focused in the mid-plane of the vessel at a major radius of 31 cm, near the predicted center of the compressed plasma, and is dumped in a plate of cobalt glass set at the Brewster angle. The scattered light is detected through a 1/2" diam. port at the vessel mid-plane, and is focused onto the entrance slit of a 5 channel polychromator designed for the purpose.[13] This instrument uses three gratings to disperse, recombine and redisperse the light so as to achieve a very high rejection ($> 2 \times 10^{10}$) of light at the ruby laser wavelength. The advantage of this method is that no special precautions need be taken to reduce the level of stray laser light in the vessel; however, the disadvantage is that Rayleigh scattering from a neutral gas cannot be used to calibrate,[14] and thus only relative density can be measured.

Small magnetic probes in alumina or quartz housing were used to measure magnetic field components during both the ionization phase and the compression phase. The probes were introduced radially at the mid-plane through the Thomson scattering viewing port for $B_\theta(R)$ and

$B_z(R)$ scans, and axially at a major radius R = 31 cm through the Thomson scattering laser dump port for $B_r(z)$ and $B_\theta(z)$ scans. The boil-off time in a plasma with density and temperature typical of the experiment is > 1 msec for alumina and $\gtrsim$ 100 μsec for quartz,[15] so the probe measurements should be reliable, at least from this point of view, for times of experimental interest. The probes consisted of two small coils (20 turns, 3 mm diam.) separated by 2 cm on one single probe structure, plus a "dummy" coil. The dummy was the same as the "real" probes except that the coil was replaced by a short. Thus three pairs of leads emerge from the probe housing, connecting to the two coils plus the dummy. The dummy allows for a test of system pick-up - if a clean dummy trace is not obtained, ground loops or other spurious signals are present and must be eliminated. Before beginning a run tests are made for system health: the dummy probe signal in vacuum and in plasma is inspected, and the probe is rotated by 180° to check that the scope signals invert without change of shape (thus indicating that the signals are magnetic in origin and not electrostatic). Having done these tests, we are confident that the signals observed are true magnetic field signals.

A Faraday cup was used as an additional temperature diagnostic. It was inserted through the pumping port in such a manner as to intercept the plasma flux escaping along the cusp open field lines. By varying the collector bias an estimate could be made of the electron energy.

Tightly wrapped around the minor cross-section of the vessel were a Rogowski coil to measure the total toroidal plasma current and a diamagnetic loop to measure the plasma pressure.

Capacitor bank charging voltages and discharge currents at various points in the electrical system were measured in the usual way.

A schematic of the entire experimental set-up is shown in Fig. 6.

IV. The Ionization Phase

A. Philosophy and Design

The principal objective of the ionization phase of Tormac V is to form a clean, highly conducting plasma with an embedded toroidal magnetic field. The ionizer must therefore ionize the neutral gas, heat the resulting plasma, and maintain the plasma in a quasi-equilibrium position away from the chamber walls.

A toroidal current is induced in the chamber to dissociate, ionize and heat the gas. The magnitudes of the current and the "vertical" field are such as to satisfy the tokamak equilibrium condition, while the curvature of the vertical field is designed to provide equilibrium with respect to R and z axis displacement. Rapid oscillation of the current inhibits the growth of helical instabilities associated with large plasma currents.

Two configurations of the pre-ionizer will be discussed. Configuration A produced a quasi-equilibrium plasma with a peak current of 40 kA. Configuration B increased the peak plasma current to 100 kA.

Two conditions related to plasma equilibrium have been considered in the design of the ionizer. The first is the ratio of plasma current to vertical magnetic field. This condition can be expressed as[16]

$$B_{\perp} = \frac{\mu_0 I_{\phi}}{4\pi R}\left[\ell n\left(\frac{8R}{a}\right) + \beta + \frac{\ell_i}{2} - \frac{3}{2}\right]$$

where

$$\ell_i = \frac{\int_0^a B_\theta^2(r) 2\pi r dr}{\pi a^2 B^2(a)}$$

and

$$\bar{\beta}_\theta = \frac{2\mu_o}{\pi a^2 B_\theta^2(a)} \int_0^a 2\pi r P(r) dr$$

where a is the plasma minor radius, R is the major radius, $B_\perp$ is the vertical field at the plasma major radius, B_θ is the poloidal field due to I_ϕ, the plama current, and P is the particle pressure. Assuming a parabolic current density distribution, $\bar{\beta}_\theta = 0.5$, and an aspect ratio of 3.5 gives

$$B_\perp = 3 \frac{\mu_o I_\phi}{4\pi R}$$

A computer code was used to determine the vacuum magnetic field by evaluating the elliptic integrals for each coil and superposing the fields. This code also gives the value of the flux function $\psi = RA_\phi$ at each grid point. The plasma current I_ϕ was determined by modeling the plasma as a set of line currents along the desired plasma boundary.

If the plasma is taken to be a perfectly conducting torus, then the amount of current generated in the plasma is just enough to keep the total flux through the center of the torus equal to the vacuum value at the plasma major radius. This current, I_ϕ, is used to calculate the necessary $B_\perp$. We therefore have an equilibrium field $B_\perp$ and a vacuum field B at the plasma major radius. The values of $B_\perp$ and B can be compared, and when they are equal, the proper equilibrium has been established. Changing the location of the toroidal coils and the ratio of currents in the various coils changes $B_\perp$ and B in different ways, so that it is possible to arrive at a solution. It should be noted that the equilibrium is no more than an extension of the betatron condition[17] to the case with large currents.

Another condition to be considered is the curvature of the vertical field. The decay index, defined as $n = -\frac{R}{B}\frac{dB}{dR}$, should be $0 < n < 3/2$ to ensure stability with respect to displacement in z and R.[16] Varying the positions and currents of the various coils changes this curvature. The computer code calculates n for each configuration so this condition can be checked.

Since there are an infinite number of configurations possible which satisfy the above conditions, one chooses among them by picking the configuration which gives the most plasma current, I_ϕ, for a given amount of bank energy. Note also that the coil locations are constrained by the size and structure of the vessel.

Another important consideration is the ringing frequency of the circuit. One would like to match the capacitance of the capacitor bank and inductances of the coils so that the quarter period $\tau_{1/4} < a/v_A$,

where $v_A = B_p/\sqrt{4\pi\rho}$. This ensures that the quarter period is less than the growth time for helical instabilities.[18]

Fig. 7a shows the coil locations for configuration A, which produced a measured plasma current $I_\phi \sim 40$ kA, with a frequency of 35 kHz. The outer coils were 1/4 turn coils, and the inner coils were 3 turn coils. The capacitor bank consisted of 2 series sections, each with four 20 kV, 14.1 μF capacitors in parallel. All switching was accomplished through ignitrons. It was necesary to put the inner and outer coils in series to avoid coupling between the pre-ionizer coils and the main cusp coils; if the inner and outer coils are in parallel, large currents are induced in these coils when the main cusp bank is fired. Also, placing these coils in series allows better control of the fields, since the ratio of fields is just a function of the size and number of turns in each coil, and does not vary as the inductance changes due to plasma current. Obviously, placing the coils in series increases the system inductance, and consequently makes higher frequencies more difficult to attain.

Fig. 7b shows configuration B, which was built to increase the amount of plasma current to 100 kA while maintaining an equilibrium configuration. The central solenoid, twenty 1-1/2 turn coils in parallel, pumps flux through the center of the torus, and, therefore, efficiently increases the plasma current without significantly increasing the vertical field at the plasma position. The capacitor bank was also modified so that it consisted of three series sections, each comprising four 20 kV, 14.1 μF capacitors in parallel. This bank thus stores more energy with less capacitance than the configuration A bank. The decrease in capacitance is necessary to increase the ringing

frequency of the system, which must increase to satisfy $\tau_{1/4} < a/v_A$, since v_A is proportional to the poloidal field, which is proportional to the toroidal current. As the toroidal current is increased the quarter period must therefore be decreased. Configuration B has a frequency of 50 kHz, and produces a maximum plasma current of ~100 kA.

Figures 8a and 8b show the vacuum field lines for configurations A and B. The computer also calculates the values of $B_\perp$, n, and the plasma current normalized for a particular amount of stored energy, I_{norm}. This normalization includes the stray inductance in the capacitor bank and the connecting cables, and so enables a standard comparison between competing coil designs.

B. Experimental Results

The plasma produced by configuration A has been examined using a number of diagnostics. These diagnostics include a Rogowski loop which measures the total plasma current, magnetic probes which measure the local poloidal magnetic field, a He-Ne laser interferometer which measures the line density in the z direction at different radii, and ruby laser 90° Thomson scattering which measures the electron temperature.

Interferometer measurements indicate the formation of an equilibrium plasma with a major radius of about 30 cm. Integrating the line density over the volume of the chamber, from a radius of 20 cm to 40 cm, show about 60% ionization for an initial fill pressure of 10 mTorr. The Rogowski loop data indicate a peak plasma current of 40 kA.

Similar data were taken for various bias fields, and the results indicate that flatter $n_e(R)$ profiles are obtained at lower bias field strengths. Fig. 9 shows the poloidal magnetic field, at a major radius

of 39 cm, as a function of time for various bias fields. The magnitude of the poloidal field distortion grows as the bias field decreases, which is consistent with the behavior of the helical instability. The flatter density profile for the low bias case is also consistent with this interpretation, since this instability tends to redistribute the plasma current and flatten the density profile. The data, therefore, indicate the probable presence of a helical instability, which is greatly reduced in magnitude by a high bias field.

Thomson scattering has been attempted on the pre-compression plasma. The signal to noise ratio was too low to obtain definitive measurements of electron temperature. Comparison with the scattering on the main Tormac plasma, and a knowledge of the electron density, enabled an estimate of $T_e < 5$ eV. This is an upper limit on the electron temperature in the precompression plasma.

The plasma produced by configuration B shows essentially the same behavior as for configuration A, except that a higher peak plasma current was established, ~100 kA, as anticipated. Also, in this case the toroidal magnetic probe data showed a quite distinct second harmonic component, indicative of an oscillatory pinching of the toroidal plasma due to the plasma current.

The ionization phase of Tormac V thus produces a quasi-stable plasma at a major radius of ~30 cm. The peak plasma current is ~40 kA or ~100 kA, depending on the coil configuration. Gross instability is minimized by oscillating the plasma current and by imposing a toroidal bias field. The electron temperature is < 5 eV.

V. The Compression Phase

A. Electron Density

The gross behavior of line density as measured by the interferometer for a typical shot is shown in Fig. 10. After the ionize bank is fired there is a delay in breakdown, determined by the gas pressure, typically a few to a few tens of microseconds; breakdown is indicated by the occurence of plasma current. After a further few tens of microseconds the line density has stabilized and the cusp bank is fired, at which time there is an increase in line density of a factor of several for interferometer locations near the plasma position, R = 30-35 cm. From data such as these and by scanning the interferometer in major radius, the profile $\int n_e d\ell(R)$ can be obtained as a function of time, and such a surface is shown in Fig. 11. Upon application of the cusp, there is an increase in line density of a factor of several at the radius of maximum increase. The location of the plasma within the vessel is about as expected from computer calculations of the field shape and position of the magnetic well, and the decay of density after the cusp field maximum has a time constant of about 20-30 μsec. Note that $\iint n_e d\ell dR$ - the area under the curves of Fig. 11, corresponding to the total number of electrons in the vessel - is not conserved, i.e., the pre-compression plasma is incompletely ionized, or there is neutral gas surrounding the main pre-compression plasma torus, and the cusp field rise creates additional plasma. The density rise seen in the data thus cannot be attributed purely to compression, but must be due to a combination of compression and additional ionization.

This general behavior of density is corroborated by measurements of Stark broadening and by Thomson scattering. The broadening of Hβ λ4861Å, if interpreted as being due purely to Stark broadening (or more specifically to Holtzmark broadening), indicates a density of $\sim 6 \times 10^{14}$ cm^{-3} before the cusp and $\sim 5 \times 10^{15}$ cm^{-3} after the cusp. However, (a) this is a line-of-sight measurement, and (b) there is reason to suspect that the post-compression line is anomalously broadened (see later, under Ion Temperature). The magnitude of the Thomson scattering signal is a reliable measure of relative electron density at a point, in particlular here at a position near the nominal center of the plasma, R = 31 cm at the midplane. Fig. 12 shows the relative density determined in this way during and just after the cusp field rise. This is consistent with the interferometer data - the density rises with the cusp and decays thereafter with a time constant ~20-30 μsec.

B. Electron Temperature

This parameter was determined in three different ways. First, the intensity ratio of the helium lines λ4686Å (He II) to λ5876Å (He I) was measured and interpreted in the manner of Griem.[19] This could be done during and after the compression but not in the pre-compression phase, since the intensity of the ionized helium line λ4686Å was then too small. During the time in which there was sufficient intensity the calculated electron temperature was ~5 eV, for all conditions under which measurements were made. This method is not expected to be very reliable, however, since the intensities are integrated along the line-of-sight and there is no guarantee that the two spectral lines originate from the same regions.

A Faraday cup was positioned in the vessel so as to intersect the cusp open field lines, as previously described. This provided a measure of the escaping plasma flux rather than of the confined plasma. The cup collector was swept in voltage and the electron temperature determined from the current-voltage characteristic so obtained. The post-compression electron temperature found in this way was ~ 7 eV, in good agreement with the line ratio measurement.

Thomson scattering provides a reliable measurement of electron temperature at a point. As for the Thomson scattering density measurements, the point of measurement here is located near the center of the main body of compressed plasma. The results of this measurement are shown in Fig. 13. The temperature is seen to reach a maximum during the rise of the cusp field and to decay away thereafter. Typically the temperature is ~ 5-10 eV, and is very insensitive to machine parameters.

C. Ion Temperature

Line-of-sight measurements of the width of the He II λ4686Å line were made. Stark broadening due to interparticle fields, and Zeeman and fine structure broadening of this line are relatively small and can be neglected compared to the measured line-width. If the line-width is ascribed to thermal Doppler and instrumental broadening, an ion temperature can be obtained. A typical time history of this temperature together with the line intensity, the electron line density, the cusp field and the ionize current waveforms is shown in Fig. 14. The temperature peaks during the cusp rise at a value ~100 eV and then decays with a time constant ~ 20 μsec. The peak ion temperature and decay time are remarkably constant, varying only in the range ~ 50-100 eV and 10-30 μsec over the wide range of operating parameters tried, viz -

filling pressure 5-50 mTorr, cusp field 2-5 kG, bias field ~200-800 G, ionize current ~ 20-100 kA, and cusp timing varied through a whole cycle of ionize current waveform.

Thus, the measured ion temperature is in strong disagreement with the Thomson scattering electron temperature, under conditions for which the ion-electron energy equipartition time is expected to be short, $\lesssim$ 1 μsec. The electron temperature obtained from Thomson scattering is known to be reliable, and is also confirmed by two other diagnostics. Some light is shed on this apparent inconsistency by the Hβ λ4861Å line shape, Fig. 15. Before compression, the Hβ line, when interpreted as being broadened by Stark and instrumental, indicates an electron density $\sim 6 \times 10^{14}$ cm^{-3}, consistent with the interferometer data. In the post-compression period the Hβ line is very broad (6.2 Å), and more importantly, shows rather distinct evidence of structure. If the width is interpreted as being due to Stark broadening corresponding to the density indicated by the interferometer, plus instrumental and Doppler broadening, then an ion temperature of ~200 eV is obtained, higher yet than the He II λ4686Å "temperature" and higher than the Thomson temperature by a factor of about 40. If the width is interpreted as being due to just Stark and instrumental, a density of $\sim 5 \times 10^{15}$ cm^{-3} is obtained, somewhat higher than that implied by interferometer data (note though that the interferometer yields a line density, and there is some uncertainty in converting this to a particle density). The presence of structure to the Hβ line, however, is indicative of the presence in the plasma of high frequency electric fields, and the broadening may thus be due to these fields rather than to the Holtzmark fields.

We conclude that the true temperature of both ions and electrons is ~ 5-10 eV, and that line-width measurements are not representative of thermal Doppler broadening. The origin of the anomalous broadening of the He II λ4686Å line is the object of further work in progress at this laboratory.[20] Parenthetically, we note that precisely this behavior - anomalously broad ion lines in the presence of a much lower Thomson scattering electron temperature - has been observed in the LASL toroidal z-pinch experiments.[21]

Further information on ion temperature is obtained from measurements of diamagentism. From shots of flux loop and cusp current signals, with and without plasma, the fractional excluded flux can be obtained. The fractional excluded flux amounts to about 2% for times at and shortly after the cusp field maximum. The proper analysis of this data requires a full accounting of the density and temperature distributions throughout the vessel, but carrying out a simpler approximate analysis yields a temperature ~10 eV, which is in good agreement with the Thomson scattering temperature. Stated otherwise, the measured apparent "temperature" as obtained from the He II λ4686Å line-width is grossly inconsistent with the measured diamagnetism.

D. Field Penetration

Magnetic probe measurements were made of the propagation of the cusp field into the pre-existing plasma. Since the probe is inserted from the larger major radius side of the plasma, where this field is primarily poloidal, we have looked mostly at $B_p(t,R;z=0)$. One way of displaying the data is to plot $B_{plasma}/B_{vac}(R,t)$ and this kind of

display, for a limited range of R, is shown in Fig. 16. Another way is to plot the time of arrival of the B_p front, for the two probe coils at various radii, and this presentation is shown in Fig. 17. These data, over a range of plasma and machine parameters, show that B_p propagates radially inwards as a front at a velocity of 3.2 cm/μsec. Measurements made using a collimated light pipe show that there is also a sharp front in Hβ light associated with the cusp firing, whose velocity of inwards propagation is 3.7 ± 0.7 cm/μsec.

The cusp field is mostly poloidal on the outside and mostly toroidal on the inside (small major radius). Having seen the poloidal component propagating inwards in major radius from the outside, one might expect to see the toroidal component propagating outwards from the inside. However, the data show that the toroidal probe signal is qualitatively different from the poloidal signal. There is no exclusion of the toroidal field; or rather, the penetration is short (compared to 1 μsec; no observable delay). There is a small "bump" on the toroidal signal, which propagates inwards at a velocity ~3 cm/μsec; we think it is likely that this feature is due to a small compression in B_T set up by the B_p propagation; this behavior has been observed by Paul et al.[22] All of these data were taken for the case of non-zero toroidal bias field, as is the normal operating condition. When the bias field is zero, however, there is an exclusion of B_T, and a propagation outwards in major radius of a B_T front at a speed of ~3 cm/μsec.

The field penetration measurements can be summarized as follows:

(i) The poloidal field component propagates inwards in major radius with a speed of ~3 cm/μsec.

(ii) There is good exclusion of B_p before the arrival of the front, and fairly complete penetration thereafter.

(iii) The B_p front is generally well defined for large major radius, but has low amplitude and poor reproducibility for $R \lesssim 30$-35 cm. (Recall that the vacuum B_p field falls off as R decreases).

(iv) The B_p front, at its sharpest, has a rise-time (10-90%) of 0.4 μsec, which at a speed of 3.2 cm/μsec corresponds to a front width of 1.3 cm. This is likely determined by the probe dimensions, but does correspond to several (2-4) ion gyroradii at $T_i = 5$ eV.

(v) The B_p front velocity approximately equals the ion thermal speed for $T_i = 5$ eV, and the sound speed for the same temperature.

(vi) There is no exclusion of the toroidal component of the cusp field, in the standard Tormac parallel bias configuration.

(vii) For the abnormal case of zero toroidal bias field, there is an exclusion of B_T for short times; B_T then propagates radially outwards from small major radius with a velocity of several cm/μsec.

Scans of the field penetration as a function of z have also been made, and the behavior is consistent with the above description. We conclude that the poloidal field is excluded for only a few micro-seconds, and the toroidal field not at all. The fast penetration of the poloidal component may indicate the necessity for a high electron temperature (low resistivity) in the pre-compression plasma. That there

is no observed exclusion at all of the toroidal field raises serious questions as to the suitability of this particular geometry (i.e., toroidal bicusp with parallel bias field) to establish the desired Tormac configuration. We note that previous experiments on pinches have shown that parallel fields fail to form a magnetic piston, even for rise-times faster than that employed here.[23,24] Our observations of field penetration in Tormac V are discussed in more detail by Feinberg et al.[25], and possible interpretations of the data proposed.

E. Shaker Heating

Shaker heating involves the launching of magnetoacoustic waves into the plasma with the expectation of their absorption in the plasma after multiple reflections from the boundary. In Tormac V, under a wide range of conditions, we observed no increase in either the line-of-sight measured apparent ion "temperature" (He II λ4686Å line broadening) or the Thomson scattering electron temperature. We also saw no significant change (i.e., $< 5\%$) in the integrated voltage-current product of the driver heating coil as plasma conditions were changed, or even when the plasma was omitted and a "vacuum shot" was made. The results were the same at low and high heater frequencies, 200-450 kHz. We conclude that the coupling to the plasma was not effective and that little or no energy was absorbed from the heater circuit by the plasma. Note that, conceptually, shaker heater requires multiple reflections from a sharp plasma boundary, and such a sharp boundary is not established in the present experiment.

VI. Summary

The observations indicate the following scenario for the plasma behavior in the Tormac V device: The gas is initially ionized to a peak density of $\sim 5 \times 10^{14}$ cm^{-3} at a temperature < 5 eV. This plasma is embedded in a pre-existing, quasi-d.c., toroidal magnetic field of strength $\lesssim 1$ kG and carries a toroidal current of peak magnitude $\lesssim 100$ kA at a frequency $\lesssim 50$ kHz. It is located in major radius near the theoretically calculated equilibrium position, R = 30 cm. We do not know with any certainty the degree of ionization of the main toroidal current-carrying plasma, but we do know that there is un-ionized gas surrounding the main plasma torus and throughout the vessel. The Tormac confinement magnetic field (the "cusp field") is switched on and rises in 13 μsec to a peak value of $\lesssim 5$ kG; at the peak it is crowbarred and it then decays with a time constant of several hundred microseconds. The plasma density (at the position of maximum density - on the midplane at a major radius ~ 30 cm) increases with the cusp field to typically $\sim 2 \times 10^{15}$ cm^{-3}. Although a part of this density increase must be due to compression, a substantial part of it is also due to ionization of residual gas by the rising cusp field, since the total number of electrons in the vessel ($\propto \iint n_e d\ell dR$, assuming toroidal symmetry) is observed to increase by a factor of several. The post-compression electron temperature is ~ 5-10 eV, and since the plasma is collisional for these parameters the ion temperature is expected to be about the same. Diamagnetic measurements of plasma pressure are consistent with the above values. After the cusp field has peaked, both the density and temperature decay with a time constant ~ 20-30 μsec. Magnetic probe

measurements show that the poloidal component of the cusp field is not well excluded by the plasma, but that it propagates radially inwards as a front with a velocity of several cm/μsec. The toroidal component of the cusp field is not excluded at all. The post-compression plasma is thus not at all as in our ideal Tormac scenario - a high β plasma torus with embedded closed field lines. Instead, after only a few microseconds the entire plasma lies on open field lines and is lost to the walls.

Our studies thus indicate that the experiment does not establish a hot plasma in the bicusp configuration.

VII. Conclusion

We have described our observations and interpretations of the Tormac V plasma behavior. The plasma formed was cold and a separation of interior plasma on closed field lines from exterior plasma on open field lines was not achieved. Thus the sought-for Tormac configuration was not established.

It is important to note that this does not imply that the Tormac concept has been invalidated. We have shown only that the method employed here of setting-up the required Tormac plasma and field geometry is inadequate. One might speculate that a higher order cusp, possessing only poloidal field components, together with a hotter, more highly ionized pre-compression plasma and a lower background gas density, might show superior behavior.[26]

VIII. Acknowledgments

We would like to thank Drs. H. L. Berk, J. W. Coonrod, M. Greenwald, W. I. B. Smith and M. C. Vella for advice and help with the experiments, and R. A. Peterson, J. Holdener, E. Salinas, G. I. Saucedo, P. D. Smith and G. L. Tabler for their technical assistance.

References

1. Berkowitz, J., Fredricks, K. O., Goertzel, H., Grad, H., Killeen, J., Rubin, E., in Peaceful Uses of Atomic Energy (Proc. 2nd Int. Conf. Geneva, 1958) 31 UN/171.
2. Combes, L.S., Gallagher, C. C., Levine, M. A., Phys. Fluids 5, 1070, (1962).
3. Boozer, A. H., Levine, M. A., Phys. Rev. Lett. 31 1287 (1973).
4. Levine, M. A., Boozer, A. H., Kalman, G., Bakshi, P., Phys. Rev. Lett. 28, 1323 (1972).
5. Brown, I. G., Kunkel, W. K. and Levine, M. A., Nuclear Fusion, 18, 761(1978).
6. Combes, L. S., Gallagher, C. C., Levine, M. A., Rev. Sci. Instr. 37, 1567 (1966).
7. We are indebted to J. Coonrod for carrying out these calculations.
8. Boozer, A. H., Bull. Am. Phys. Soc. 19, 928 (1974).
9. Levine, M. A., Gallagher, C. C., Boozer, A. H., Bull. Am. Phys. Soc. 19, 928 (1974).
10. Lietti, A., Rev. Sci. Instr. 40, 473 (1969).
11. Coonrod, J. W., Bull. Am. Phys. Soc., 21, 844 (1976).
12. Coonrod, J. W., PhD. Thesis, LBL-8167 (Sept. 1978).
13. Greenwald, M. and Smith, W. I. B., Appl. Optics 16, 587 (1977).
14. See, however, "Rotational Raman Calibration of Thomson Scattering", Howard, J., James, B. W. and Smith, W. I. B., J. Phys. D.,12, 1435 (1979), for an alternative calibration method.
15. Lovberg, R. H., in "Plasma Diagnostic Techniques", ed. Huddlestone, R. H. and Leonard, S. L. (Academic Press, New York, 1965), p. 106.

16. Mukhovatov, B. S. and Shafranov, V. D., Nuclear Fusion 11, 605 (1971).

17. Kerst, D. W. and Serber, R., Phys. Rev. 60, 53 (1941).

18. Shafranov, V. D. in Plasma Physics and the Problem of Controlled Thermonuclear Reactions", Vol. IV (Pergamon, New York, 1960), p. 71.

19. Griem, H., "Plasma Spectroscopy" (McGraw-Hill, New York, 1964) p. 274.

20. Shaw, R. S., Coonrod, J., Greenwald, M., Levine, M. A., Myers, B. R., and Vella, M. C., "Observation of Anomalously Broad Gaussian HeII 4686A Spectral Lines in Tormac," Lawrence Berkeley Laboratory Report LBL-10218; to be published in Plasma Physics.

21. Forman, P. R., private communication.

22. Paul, J. W. M., Parkinson, J. J., Sheffield, J. and Holmes, L. S., Proc. of VII Conf. on Ionization Phenomena in Gases, Belgrade (1965), p. 819.

23. DeSilva, A. W., Dove, W. F., Spaulding, I. J., Goldenbaum, G. C., Phys. Fluids 14, 42 (1971).

24. Little, E. M., Quinn, W. E., and Ribe, F. L., Phys. Fluids 4, 711 (1961).

25. Feinberg, B., Vaucher, B. G., Shaw, R. S. and Vella, M. C., "Anomalous Toroidal Field Pentration in Tormac V," Lawrence Berkeley Laboratory, Report LBL-10318; to be published.

26. Vella, M. C., Feinberg, V. and Niland, R. A., "A Shock Heated Tormac Experiment," Lawrence Berkeley Laboratory Report UCID-8059 (1978).

FIGURE CAPTIONS

Fig. 1. The Tormac bicusp plasma configuration.

Fig. 2. Tormac V vacuum vessel and calculated plasma location and field shape.

Fig. 3. Cross-section of vacuum poloidal flux surfaces.

Fig. 4. Cross-section of vacuum magnetic field intensity.

Fig. 5. Plot of vacuum $|B|$ versus major radius at the midplane.

Fig. 6. Diagnostics and banks for the experiment.

Fig. 7. Coil locations for ionizer configuration A (7a) and B (7b).

Fig. 8. Cross section of vacuum poloidal fields for ionizer configurations A (8a) and B (8b).

Fig. 9. Ionize current and poloidal magnetic field at R = 39 cm as a function of time for various toroidal bias fields. The magnitude of the poloidal field distortion grows as the bias field decreases.

Fig. 10 Typical interferometer measurement of line density.

Fig. 11. Interferometer measurements. The surface shows $\int n_e d\ell$ as a function of R for time slices before, during and after application of the cusp field, B_{cusp}.

Fig. 12. Thomson scattering measurements of electron density as a function of time (12a) and of cusp field strength (12b).

Fig. 13. Thomson scattering measurements of electron temperature as a function of time (13a) and of cusp field strength (13b).

Fig. 14. Time history of ion "temperature" ((He II) λ4686Å line broadening), He II λ4686Å line intensity, electron line density, cusp field strength, and ionize current.

Fig. 15. Hβ λ4861Å line shape before and after application of the cusp field.

Fig. 16. Poloidal magnetic field as a function of major radius at different times after firing of the cusp field.

Fig. 17. Arrival time of the poloidal magnetic field front versus major radius.

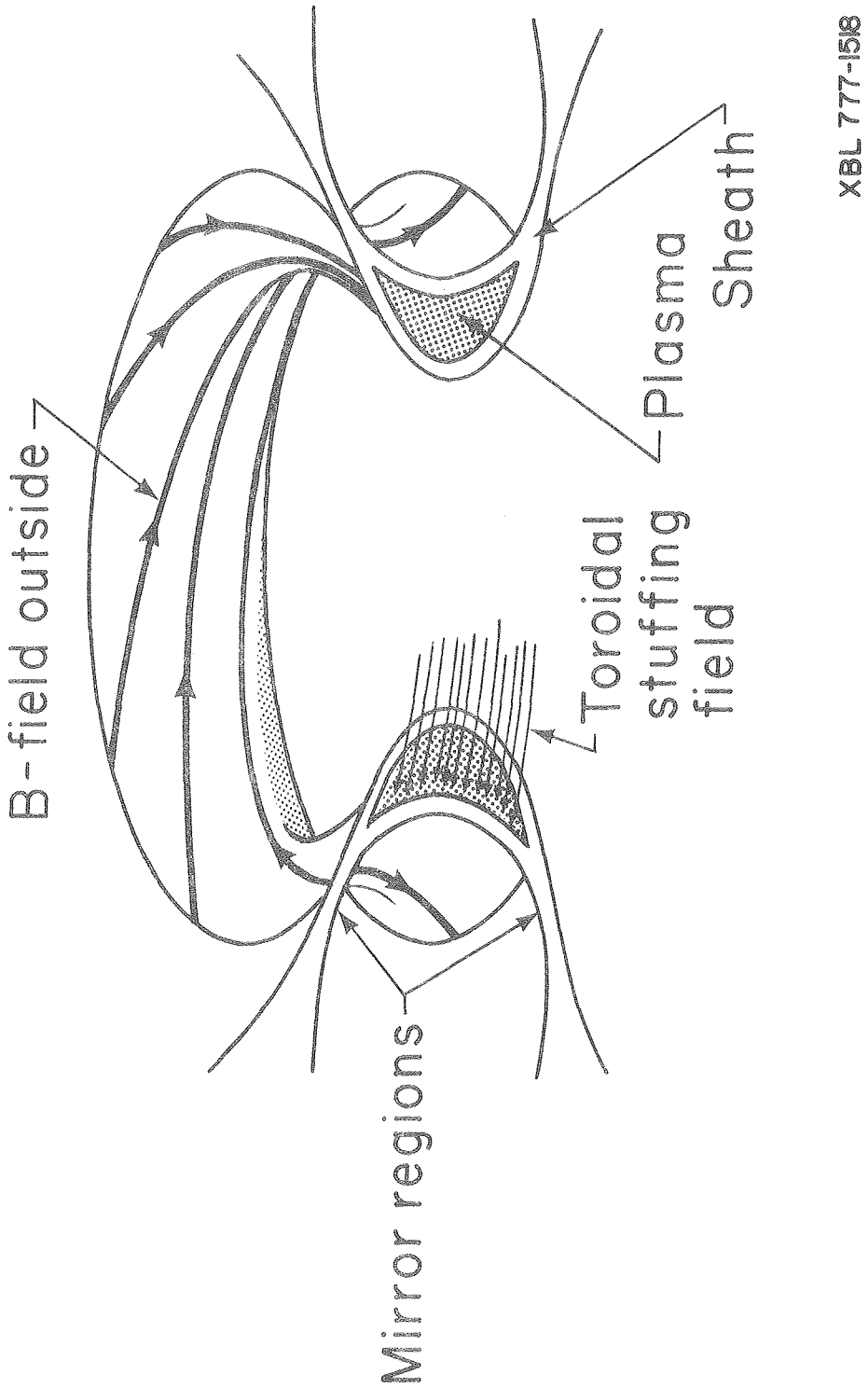

XBL 777-1518

Fig. 1

Plasma disposition within vacuum vessel

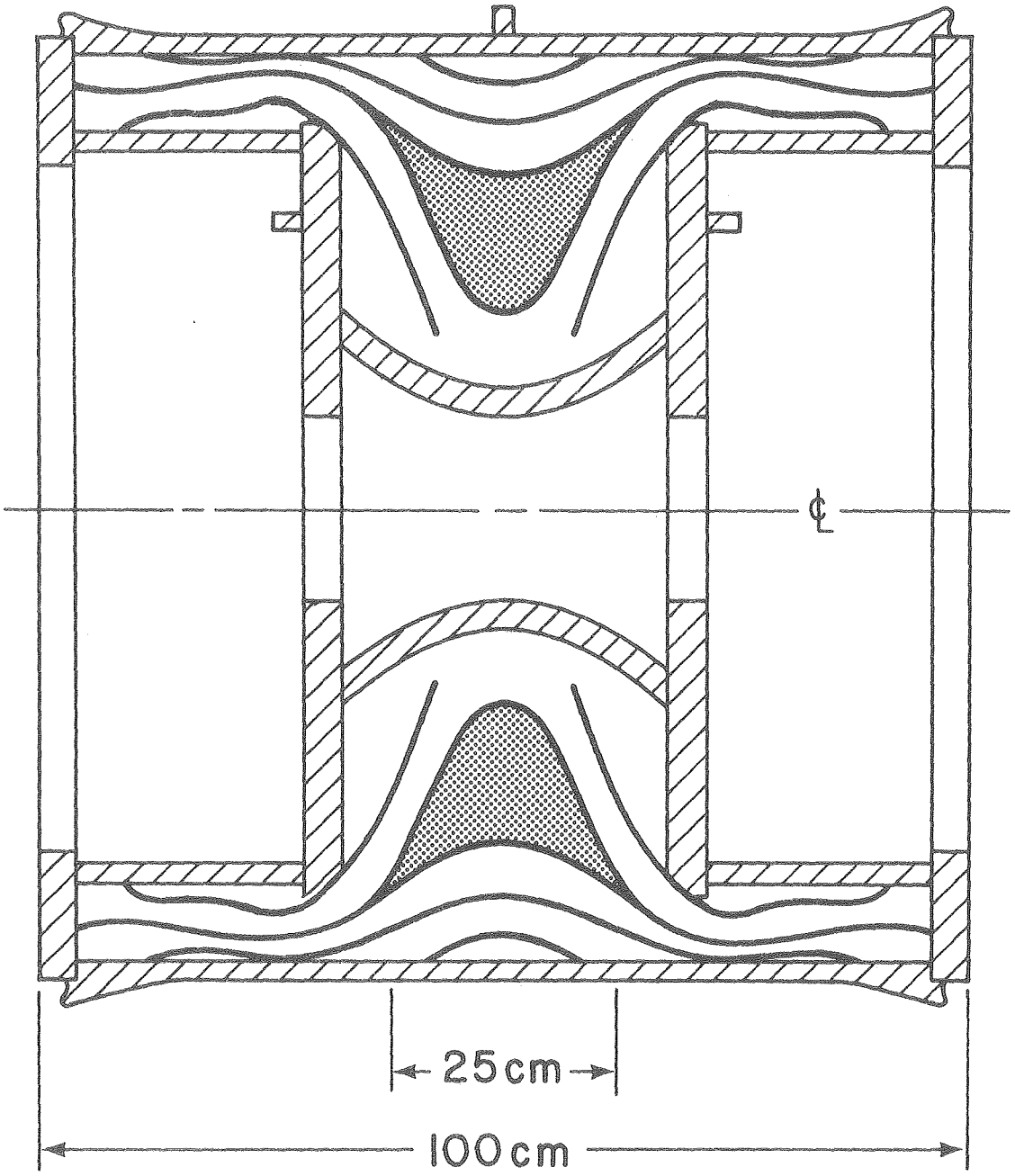

Fig. 2

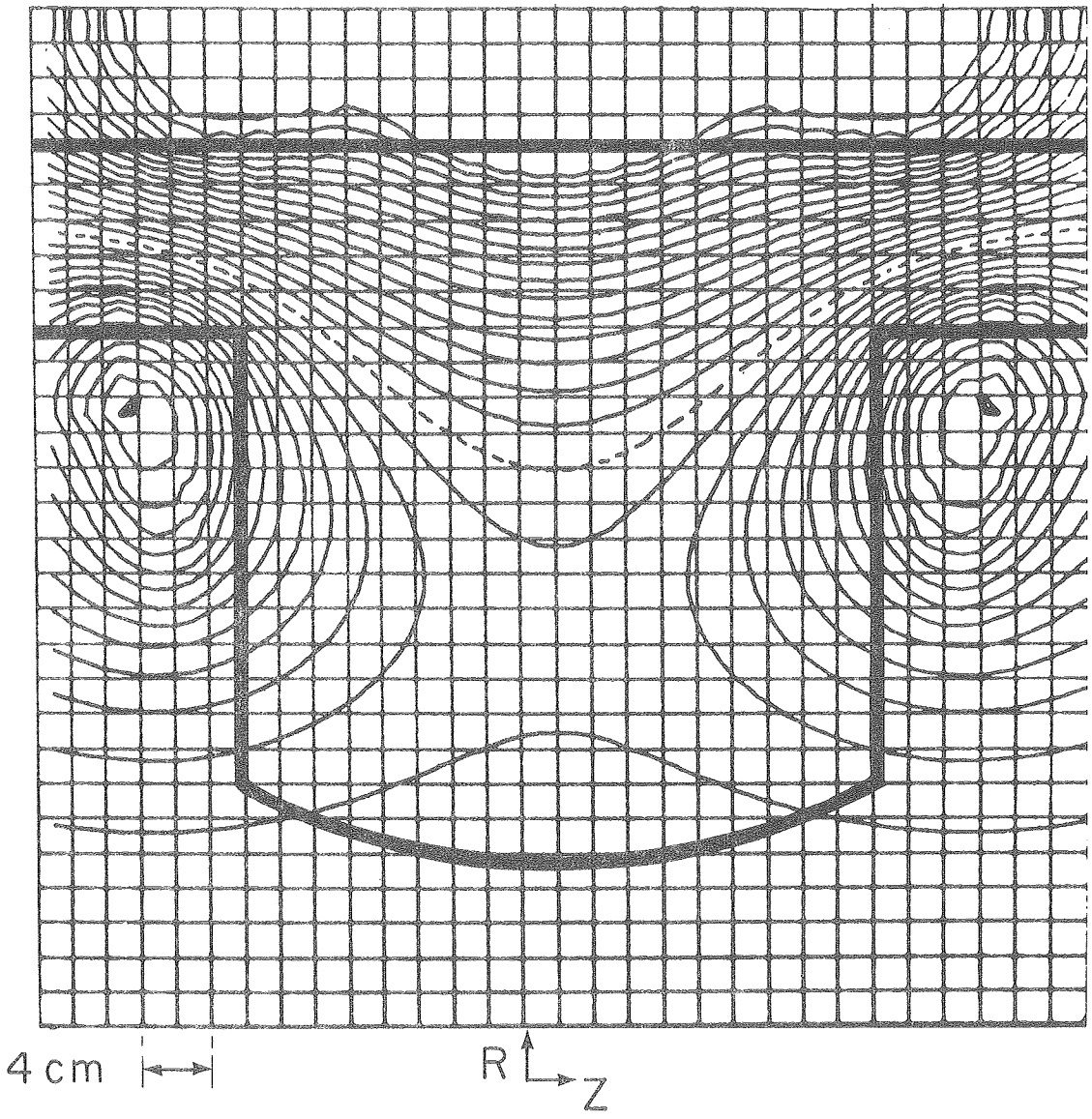

XBL 805-1109

Fig. 3

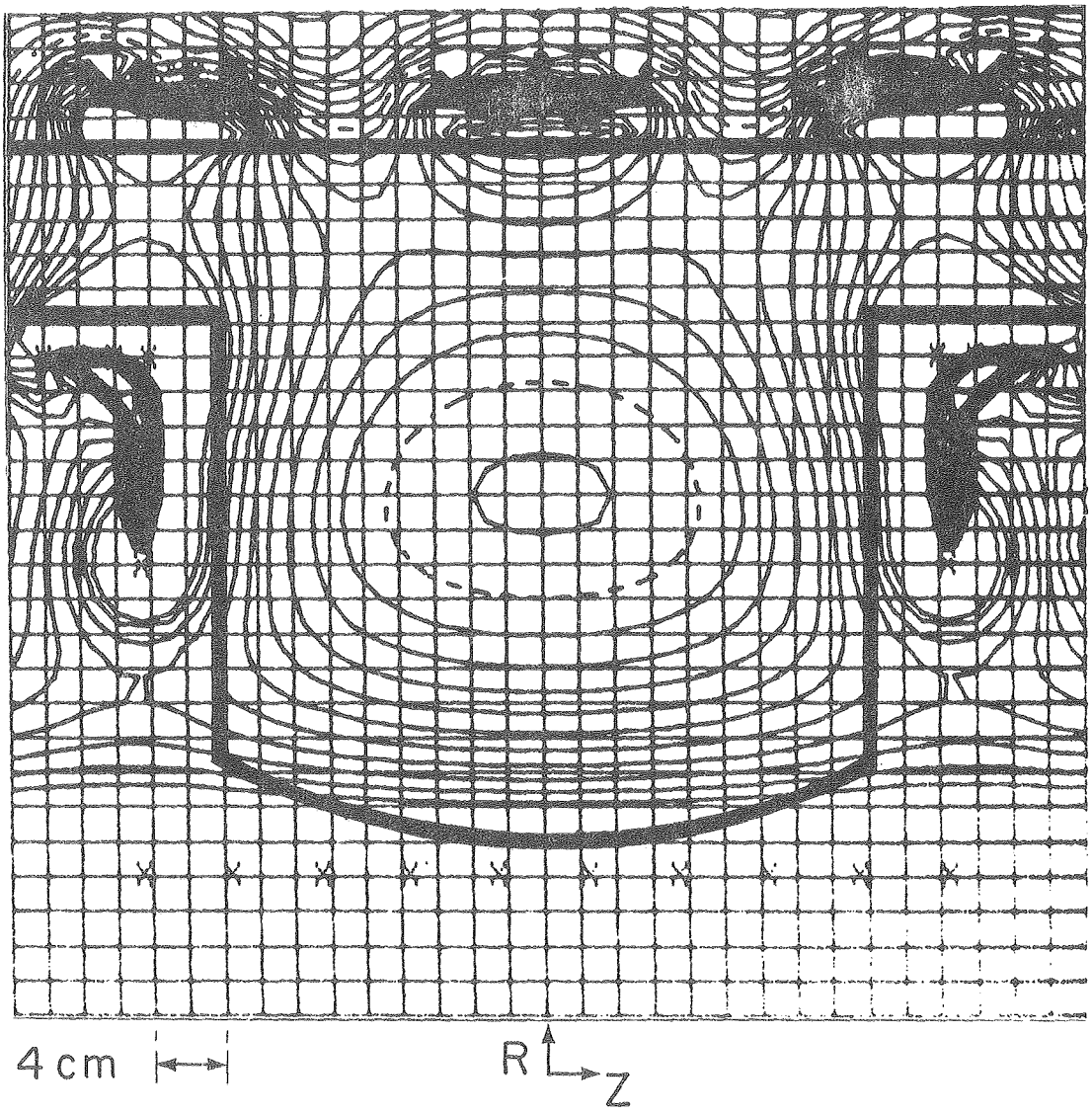

XBL 805-1108

Fig. 4

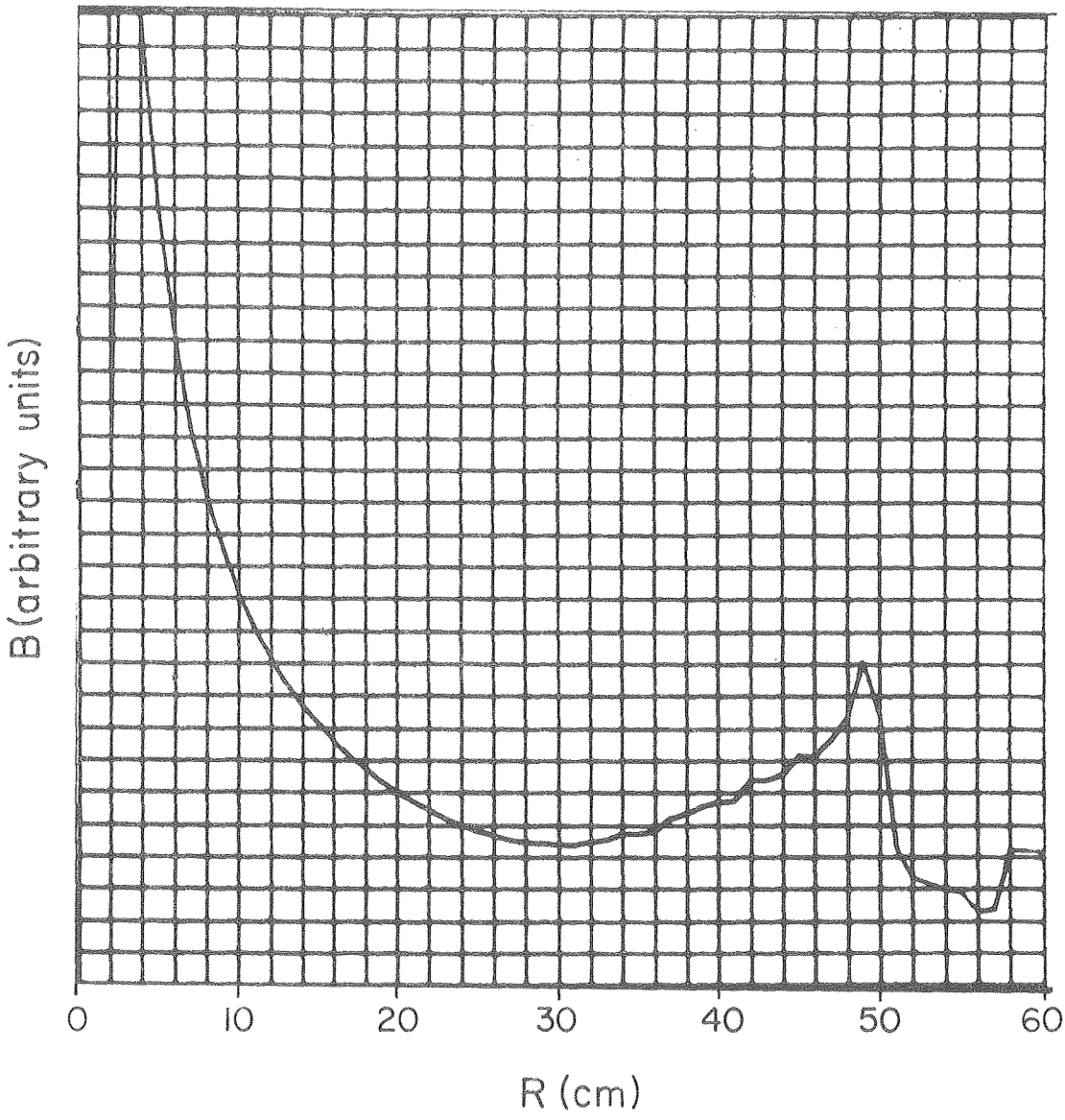

XBL 804 – 688

Fig. 5

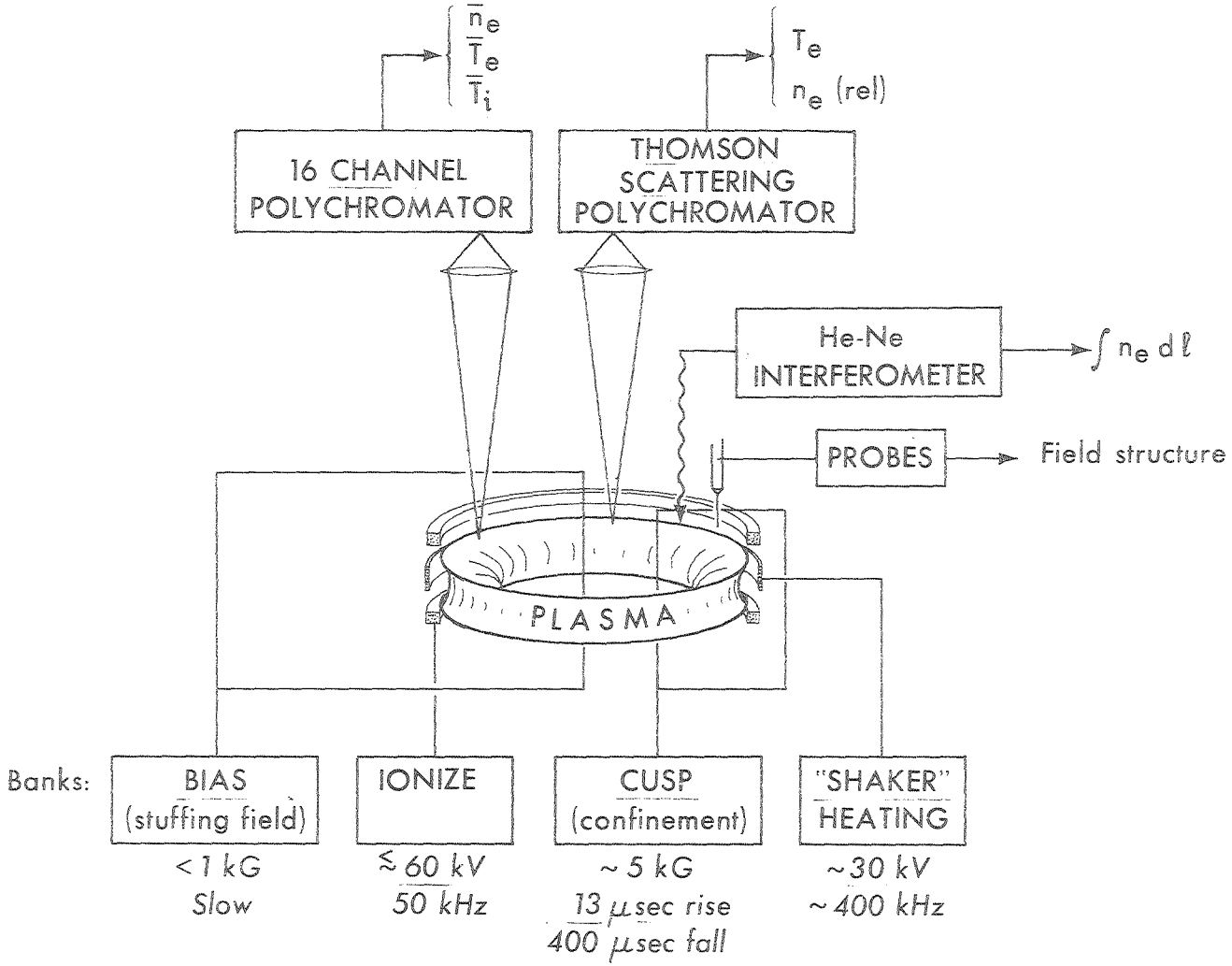

XBL 7510-8605A

Fig. 6

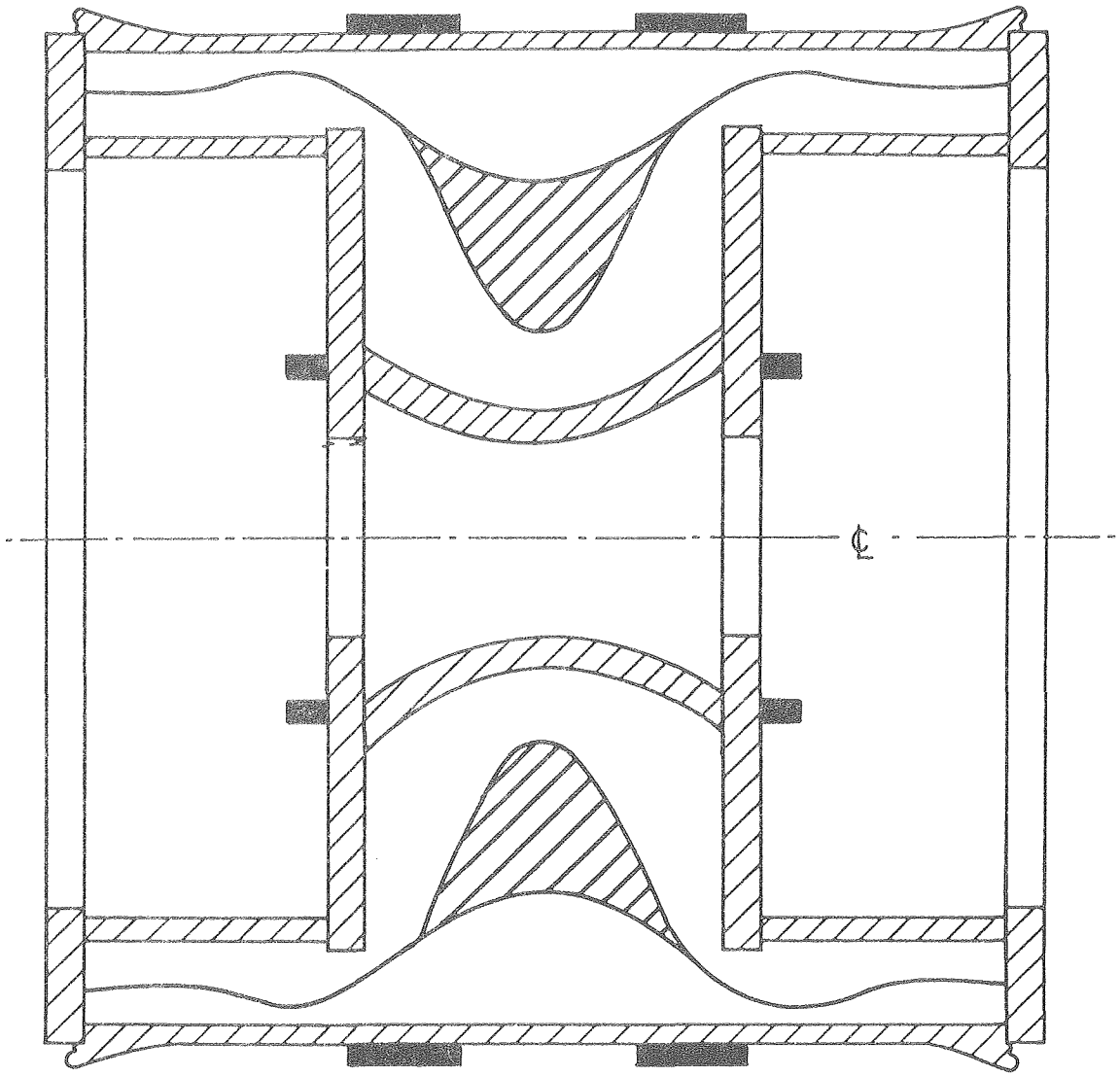

XBL 757-4469B

Fig. 7(a)

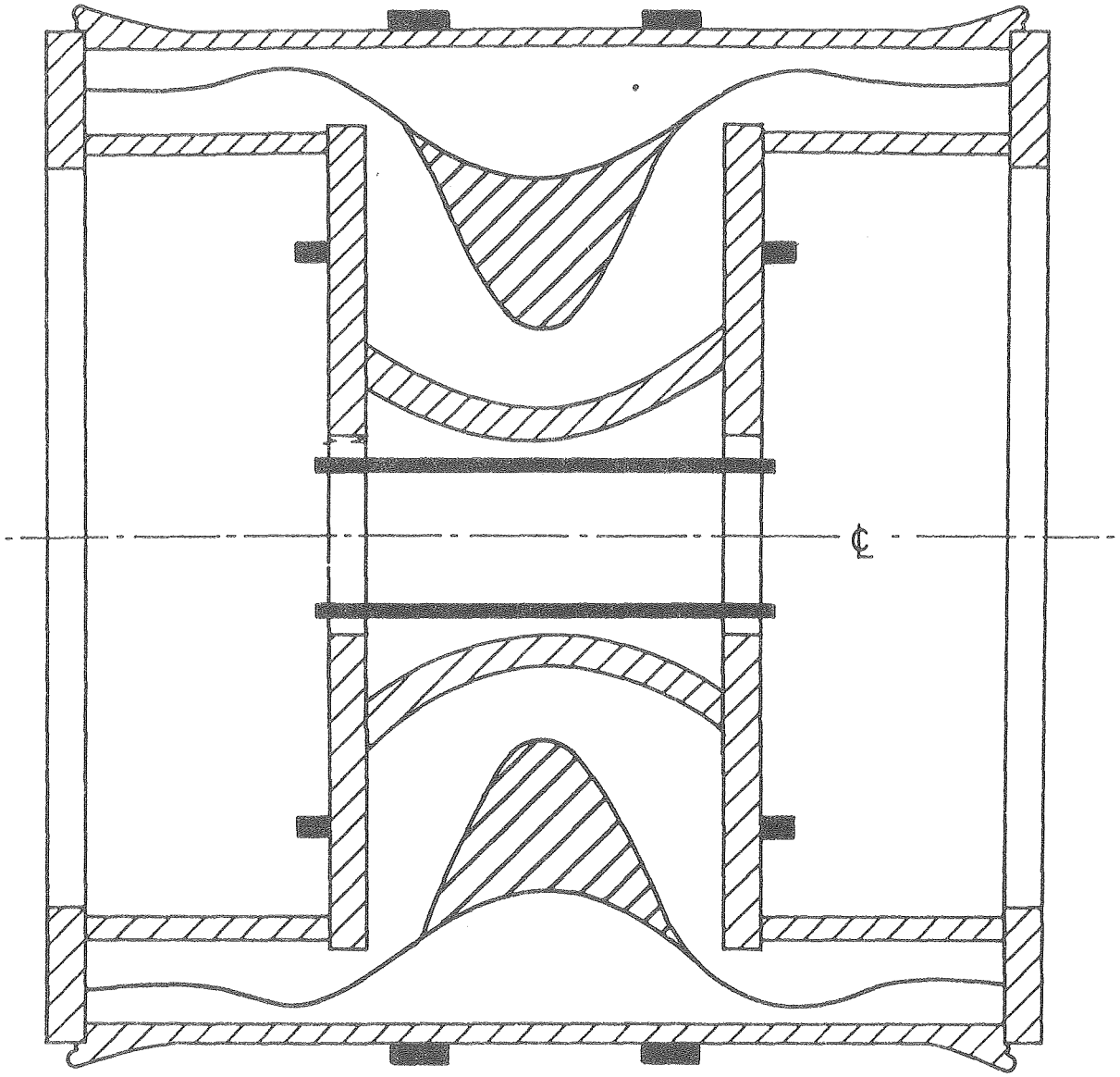

XBL 757-4469A

Fig. 7(b)

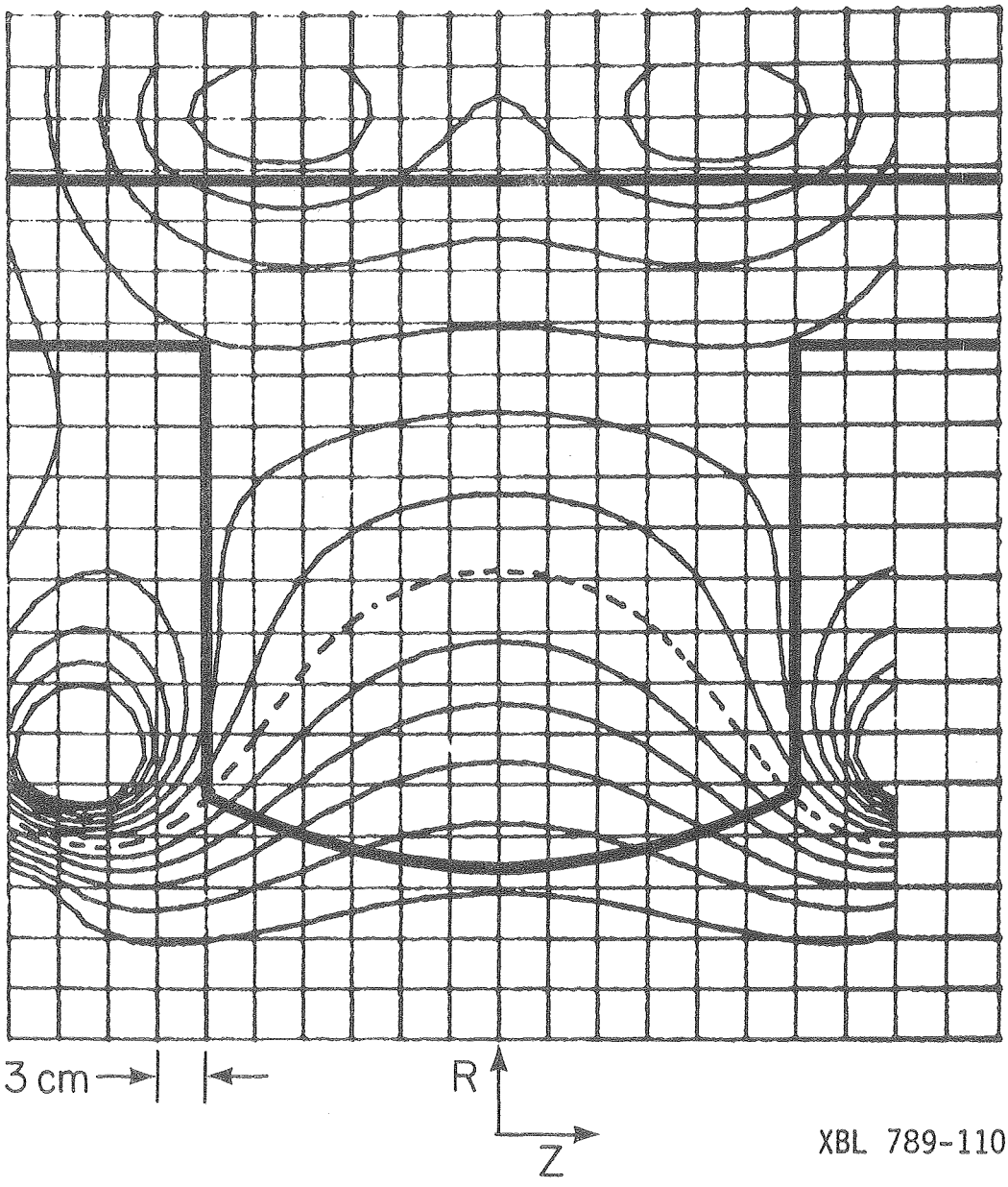

Fig. 8(a)

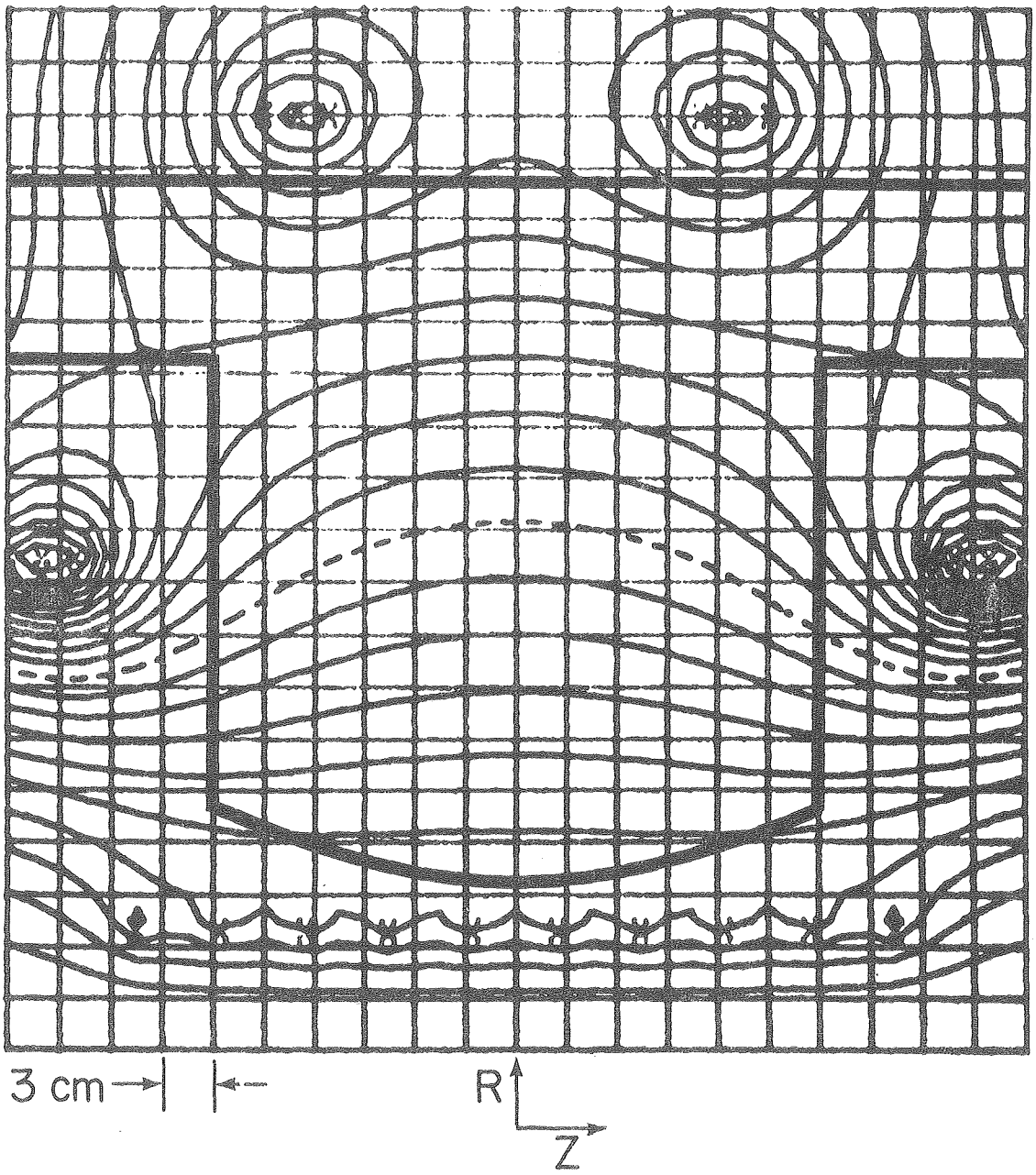

XBL 806-1173

Fig. 8(b)

Ionize current

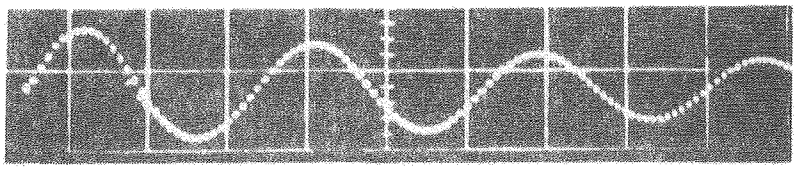

10 μsec/cm

Poloidal magnetic field

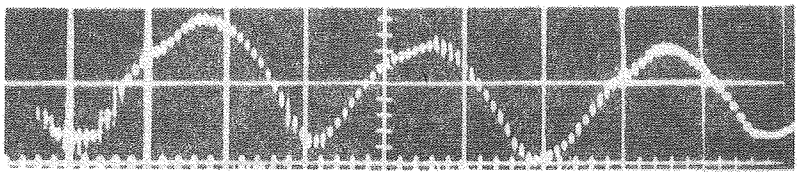

B_T = 750G

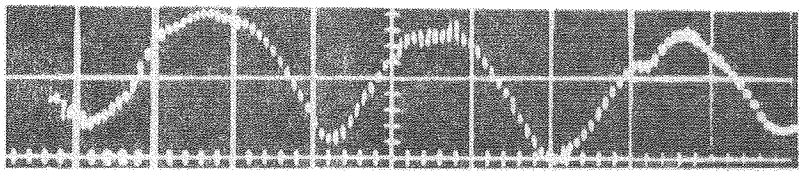

B_T = 562G

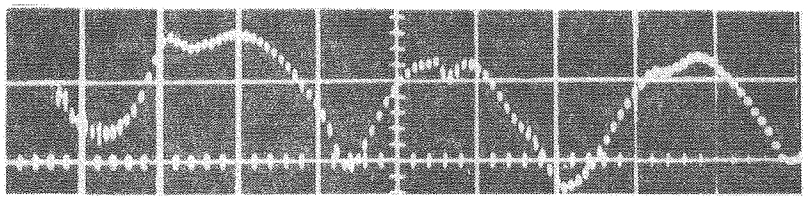

B_T = 375G

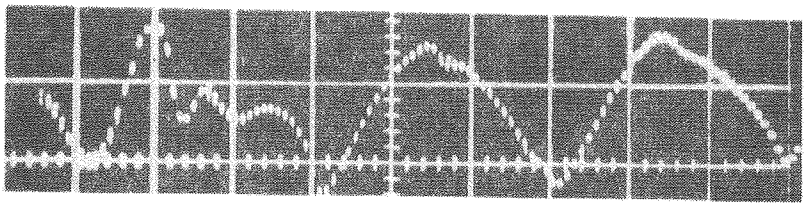

B_T = 187G

Fig. 9

XBB804 5055

Tormac V Interferometer Measurements

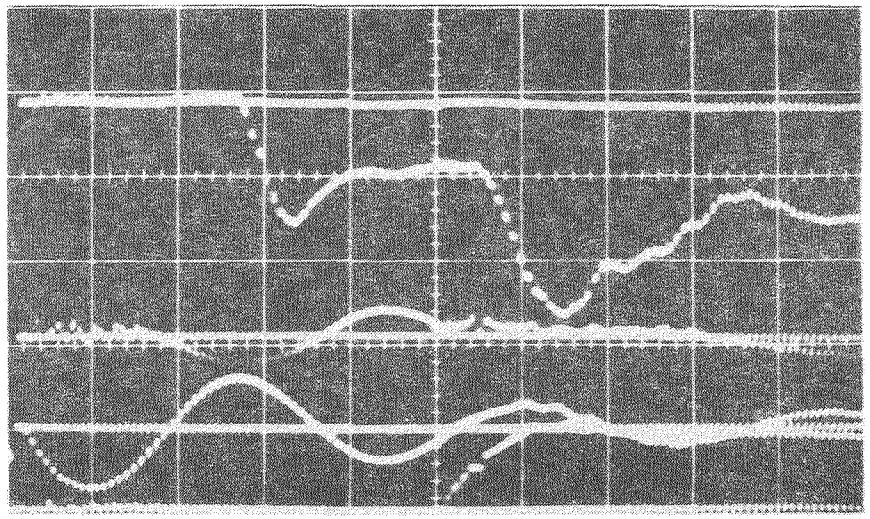

XBB804 5056

Fig. 10

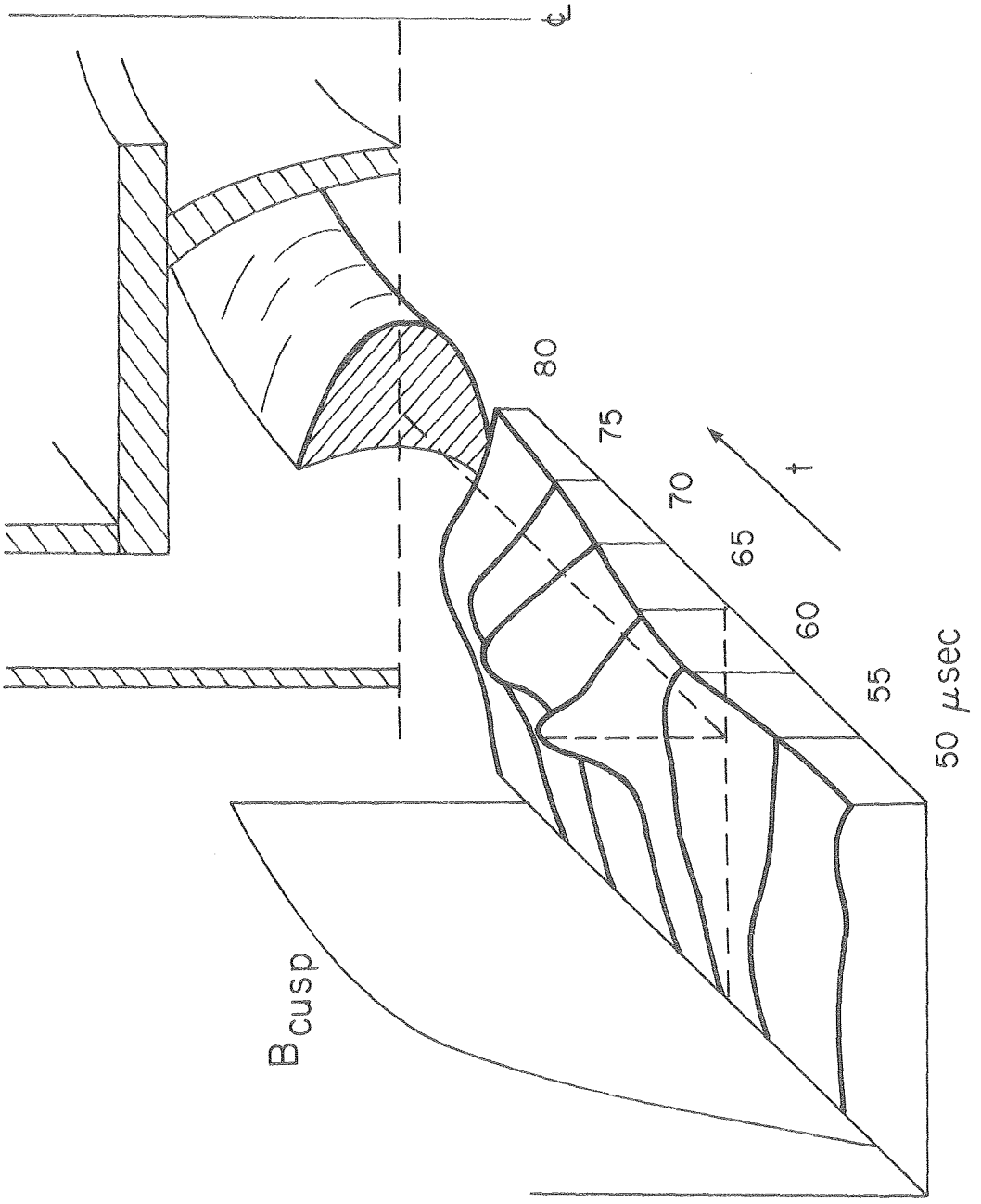

XBL 787-1405A

Fig. 11

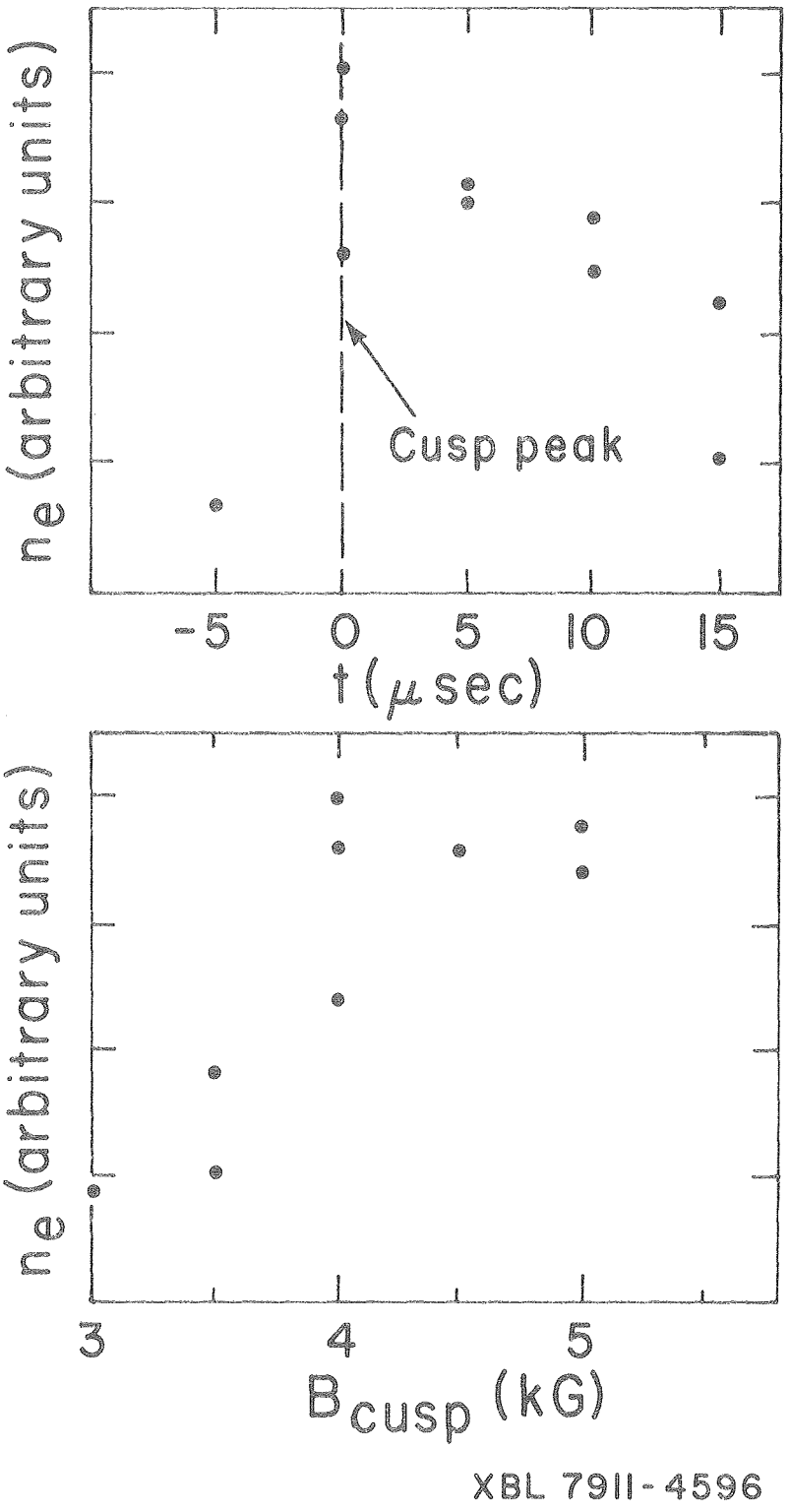
ne (arbitrary units)
Cusp peak
-5
0
5
10
15
t(μsec)
ne (arbitrary units)
3
4
5
Bcusp (kG)
XBL 7911-4596

Fig. 12

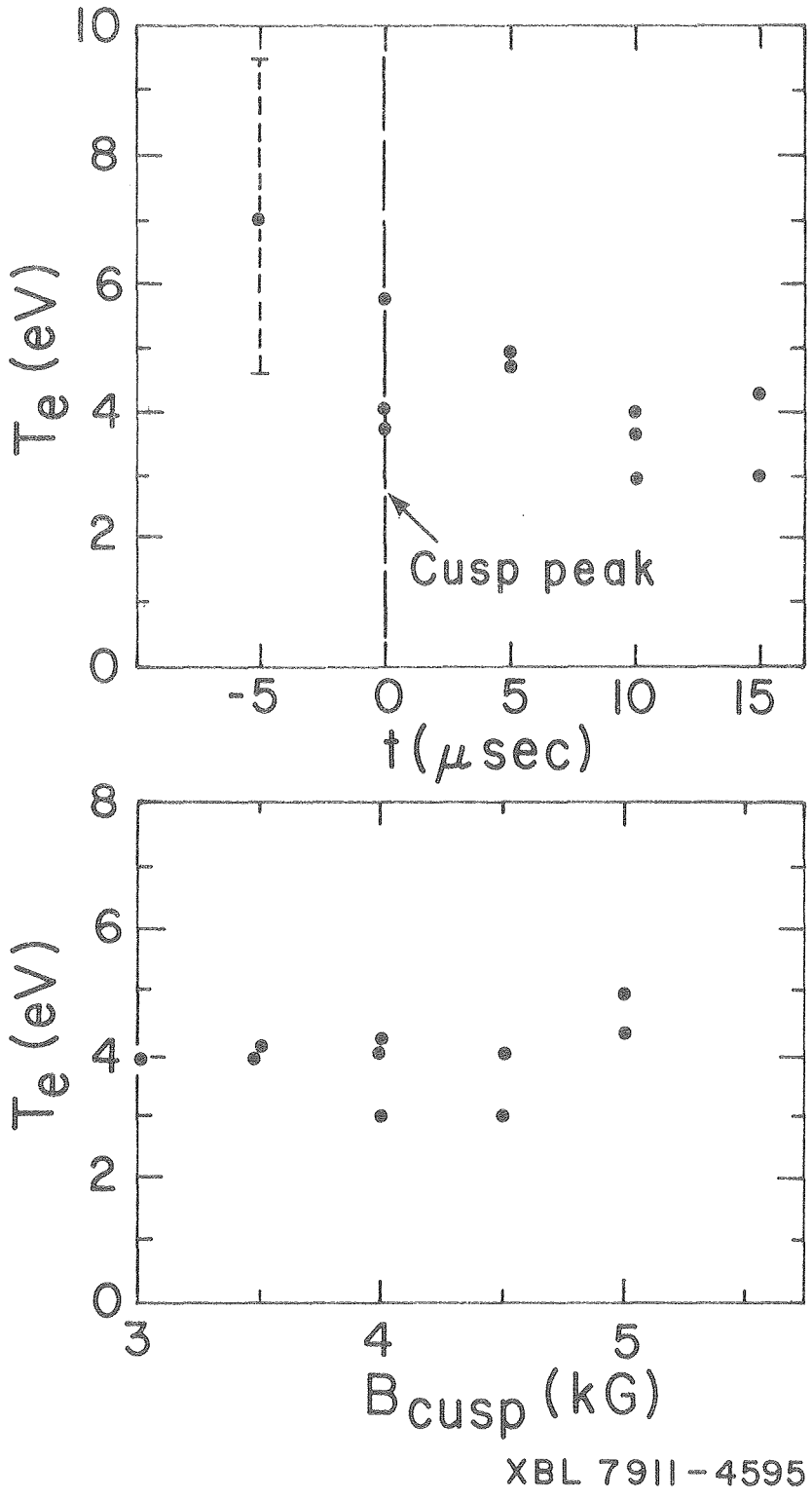
Te (eV)
10
8
6
4
2
0
-5
0
5
10
15
t(μsec)
Cusp peak
Te (eV)
8
6
4
2
0
3
4
5
Bcusp (kG)
XBL 7911-4595

Fig. 13

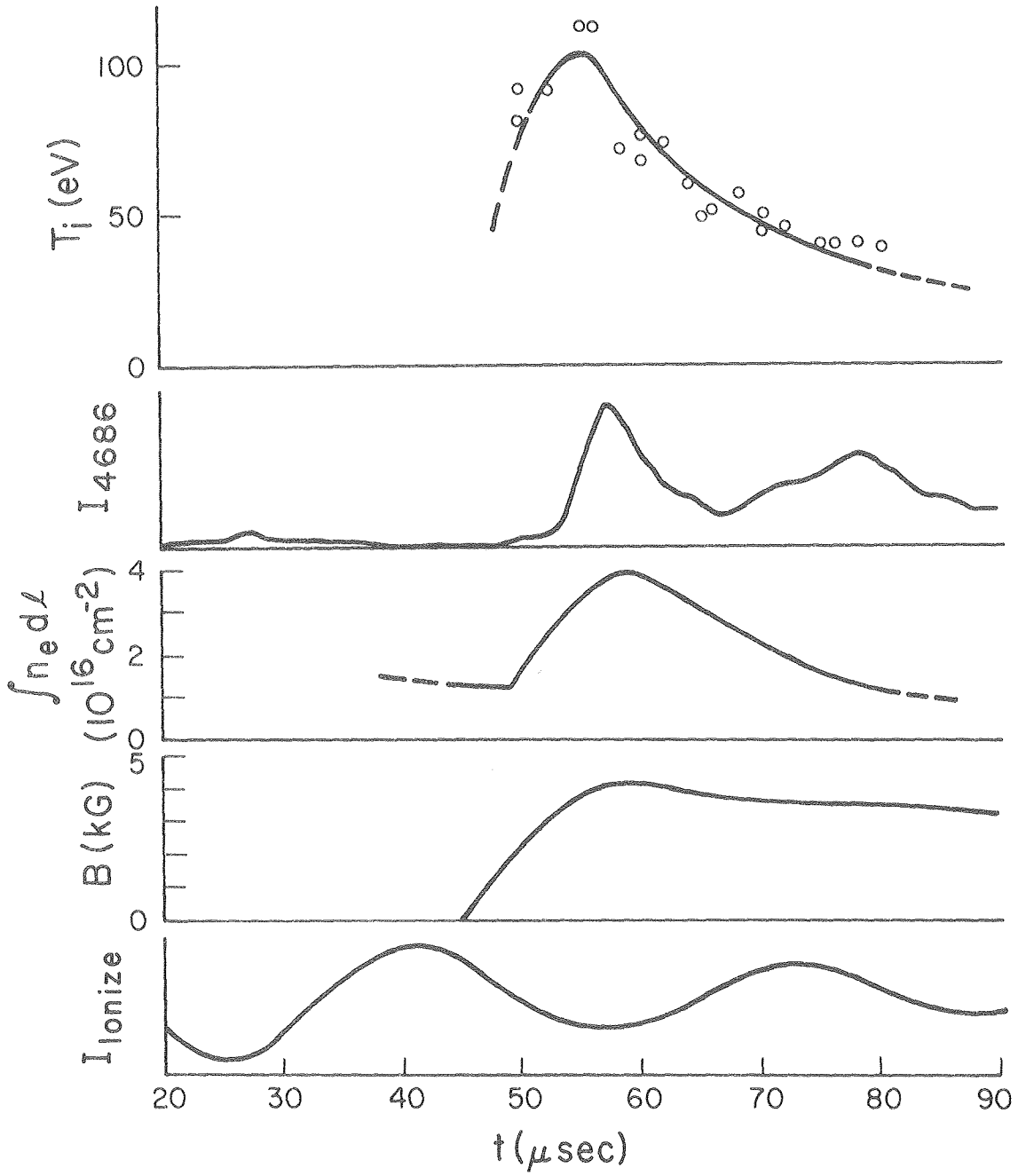

XBL 787-1407

Fig. 14

H_β Line broadening

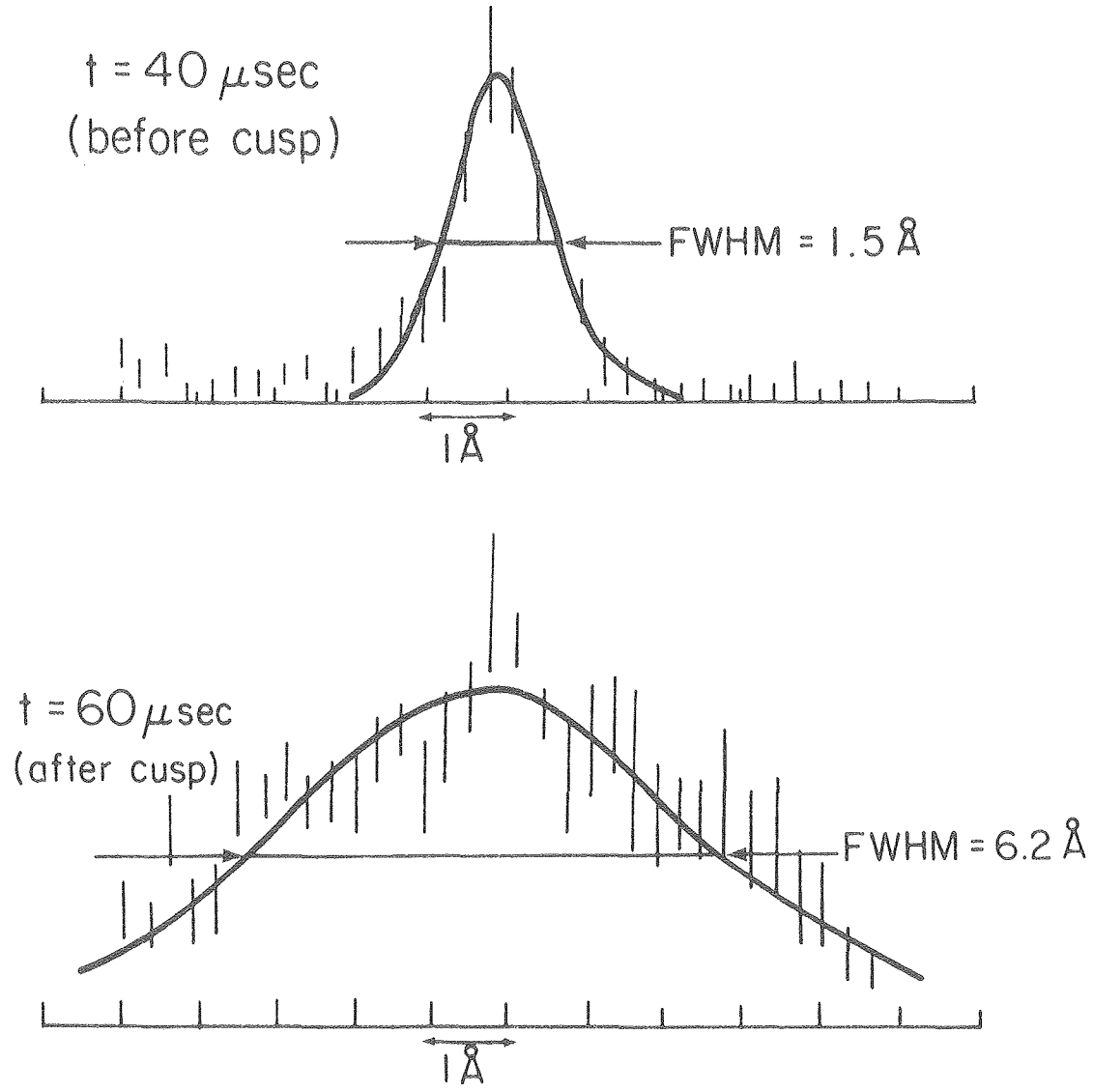

XBL 787-1387

Fig. 15

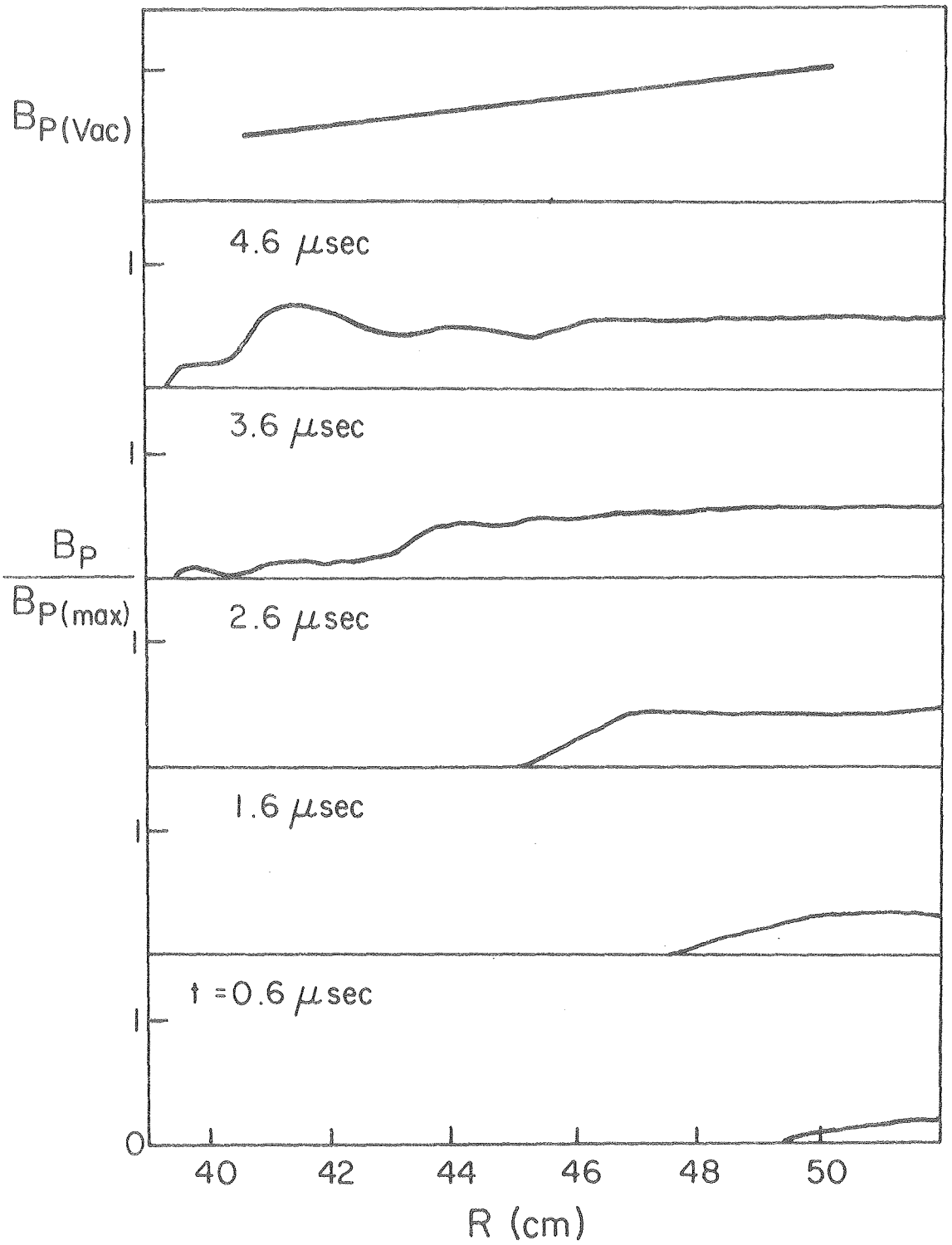

XBL 787-1388

Fig. 16

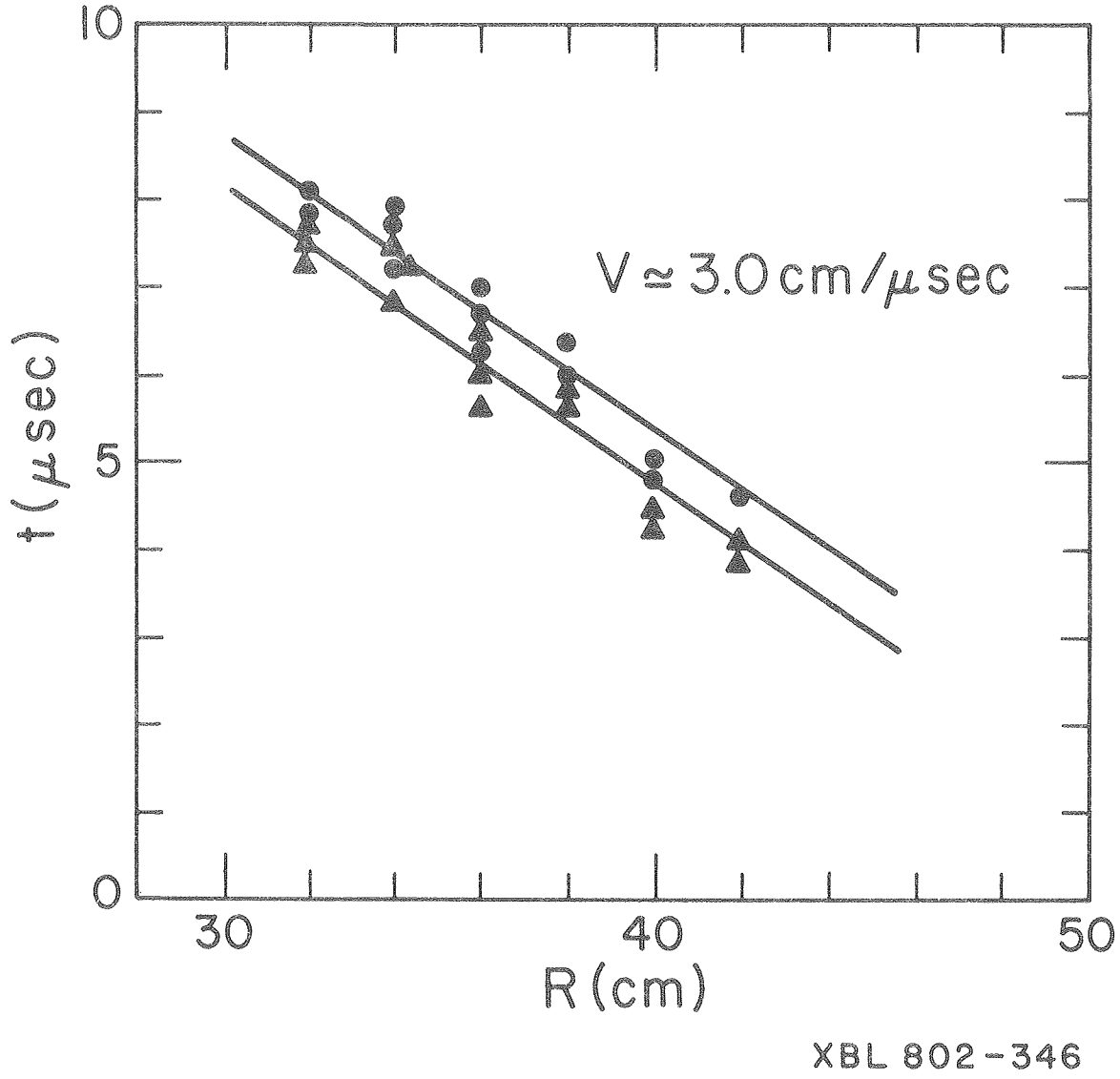

Fig. 17